Journal of Pharmaceutical Innovation (2026) 21:517
https://doi.org/10.1007/s12247-026-10698-5

RESEARCH

# Phytochemical Characterization and in Silico Evaluation of Bioactive Compounds from *Passiflora quadrangularis L.* Against 17B-HSD1

**Gopika V C[1] · Jayashree V[2]**

Received: 28 July 2025 / Accepted: 13 April 2026


## Abstract

**Background** *Passiflora quadrangularis L.* is a plant with a rich phytochemical profile that has been reported to exhibit neuroprotective, cardioprotective, and anticancer effects. Its molecular mechanisms and bioactive compounds are, however, not well characterized.

**Objective** The purpose of the study was to determine the phytochemical profile of *P. quadrangularis* leaves, isolate prominent flavonoids, and determine the anticancer properties of these flavonoids on *17β-Hydroxysteroid Dehydrogenase Type 1* through in silico methods.

**Methods** Ethanolic extracts were quantitatively screened by phytochemical screening and column chromatography to isolate their compounds. FTIR, NMR, and mass spectrometric analysis were conducted to elucidate the structure. *AutoDock Vina* was used to perform molecular docking and molecular dynamics with *GROMACS* to determine the stability of binding.

**Results** Phenolics (305 mg/g), flavonoids (296 mg/g) were found in high levels. Quercetin and kaempferol are two key compounds that were identified successfully. The outcomes of docking indicated that it had a strong binding affinity to the target 17B-HSD1 (−9.5 kcal/mol) and the presence of a high interaction with HER2, STING, and PARP10 targets. Molecular dynamics simulations showed that there were stable ligand-protein interactions, where there was minimal structural deviation and hydrogen bonding.

**Conclusion** The results show that the flavonoids of *P. quadrangularis* have promising anticancer properties, with multi-target effects, especially by regulating estrogen metabolism pathways, and can be further used as lead compounds in drug discovery.

**Keywords** Passiflora quadrangularis L. · Phytochemical profiling · 17β-HSD Type 1 · Molecular docking · Molecular dynamics simulation

## Introduction

Natural products have long been at the forefront of drug discovery, offering a structurally diverse array of bioactive compounds that continue to shape therapeutic innovation. Phytochemicals offer a valuable source of new agents targeting mechanisms, often in malignancies where multifactorial pathologies indicate the need for multi-target agents. Herbal medicines, which exist as sub-streams of traditional healing systems, are relevant as a resource of bioactive compounds, many of which are now approved agents. Among the genus Passiflora, *Passiflora quadrangularis L.* or giant granadilla, has emerged as an invaluable pharmacological resource owing to its phytochemical diversity and biological activity [1, 2].

Phytochemically, *P. quadrangularis* is a prolific source of secondary metabolites including flavonoids, phenolic acids, alkaloids, triterpenoid saponins, and cyanogenic glycosides. In particular, flavonoid derivatives like apigenin, vitexin, isovitexin, orientin, luteolin and myricetin were isolated from the pericarp and leaves of the source species providing their

✉ Jayashree V
vjayashree@gmail.com

Gopika V C
gopikajinto@gmail.com

[1] School of Pharmaceutical Sciences, Deemed University Vels Institute of Science, Technology & Advanced Studies (VISTAS), Chennai, Tamil Nadu 600117, India

[2] Department of Pharmacology, Deemed University Vels Institute of Science, Technology & Advanced Studies (VISTAS), Chennai, Tamil Nadu 600117, India

Published online: 14 May 2026

antioxidant and neuropharmacological effects [3]. Also, the presence of malvidin derivatives and polyphenols bound glycosidically was confirmed by high resolution chromatographic and spectrometric techniques [4]. The finding of new cyanogenic glycosides including diastereomers [5], along with triterpenoid saponins with vasodilatory activity, expands the chemical novelty of the species even further [6, 7].

This biochemical complexity leads to a broad pharmacological range. This plant has a strong antioxidant ability, mainly due to their high level of phenolic compounds, especially in organic crops, which have been demonstrated to trigger secondary metabolite biosynthesis as a response to stresses [8, 9].

One of the most widely studied pharmacological effects of *P. quadrangularis* is its central nervous system impact. The sedative and anxiolytic properties are mediated through GABAergic modulation which is attributed mainly to the apigenin and vitexin derivatives [10]. Sedative and anxiolytic effects have been confirmed in preclinical models of ethyl ether-induced hypnosis and the elevated plus-maze with plant extracts showing similar effectiveness to standard anxiolytics (such as diazepam), consistent with its traditional use for mental calmness and insomnia treatment. Neuroprotective and memory-enhancing effects have been observed in animal models which further confirms its use [11].

*P. quadrangularis* has also been observed to have significant cardioprotective effects beyond its neuroactive actions. Several examinations have corroborated its effects on pressure related to blood, particularly from its potential to prevent vascular remodeling and activate the nitric oxide pathway in hypertensive models [12]. Ethanol and aqueous extracts formed noticeable decrease in systolic and diastolic blood pressures, validating its ethnomedicine use, with/truthful to use cardiac disease. The vasodilatory, and antihypertensive effects came from triterpenoid saponins, and a potential flavonoid-induced endothelium-dependent reduction of hypertension.

An especially intriguing pharmacological aspect of *P. quadrangularis* is the potential for its anticancer effects. Many studies have shown its cytotoxicity towards numerous tumor cell lines, including Ehrlich's ascites carcinoma and Dalton's lymphoma ascites [13, 14]. The phytochemicals from *P. quadrangularis* have been reported to act on important oncogenic signalling pathways, including induction of apoptosis, hormone receptor signalling, inhibition of DNA repair, and immune boosts. Besides, molecular docking studies have indicated that the flavonoids from *P. quadrangularis* inhibited efflux transporters, including P-glycoprotein, which highlights the potential to overcome multidrug resistance, a significant challenge in cancer chemotherapy [15].

Additional pharmacological assessments have shown antimicrobial, anti-inflammatory, anticholinesterase, and antidiabetic activities [16, 17].

These activities complement its evolving role in ethnopharmacology and modern herbal formulations. Studies on the hemolytic and dermal effects of leaf extracts indicate its potential use as a topical application and caution for systemic use, as it can express dose-dependent toxicity [17, 18]. All of these data demonstrate that *P. quadrangularis* could be considered a phytotherapeutic agent with multi-systemic uses, including neurological, cardiovascular, oncological, and dermatological uses.

There are potentially greater than what has been developed so far with *P. quadrangularis's* therapeutic properties, and its constituents of pharmacodynamic mechanisms are only partially understood regarding molecular interactions with relevant biological targets. Thus, emerging computational approaches like molecular docking and dynamic simulations delineate a useful engagement for rationalizing bioactivities at molecular levels and identifying additional lead compounds for drug development. The methodological approach taken in this study, including phytochemical investigation, compound isolation, followed by in silico modeling of compounds at the molecular level, shows the importance of integrating ethnobotany and forms of drug designs that modern scientific advancements have produced to capitalize on the true therapeutic potential that many forms of therapeutic plants can provide.

Therefore, the present study focuses on the phytochemical research of Passiflora quadrangularis L. and the analysis of its key flavonoids on the cancer-related molecular targets, especially 17β-HSD type 1, through in silico methods.

## Materials and Methods

### Plant Material

In June of 2023, Leaves of *Passiflora quadrangularis L.* were gathered in Thrissur District, Kerala, India. The plant material was found authentic at the Kerala Forest Research Institute (KFRI), Peechi, Thrissur, and a voucher specimen (Accession No. 18371) was stored to be used in the future. The sampling was done under conditions of normal weather in the area during the early monsoon. The gathered leaves were washed and dried at room temperature and kept in airtight containers till further use. Recording the time of collection is necessary because phytochemical composition can be different because of seasonal and environmental variations.

### Extraction

Soxhlet extraction with 90% ethanol was repeated on the powdered *Passiflora quadrangularis* to extract. A rotary evaporator was used to combine the extracts under reduced

pressure and filter the combined extracts at a controlled temperature. The concentrated extract was dried again to get a crude residue. This dry extract was prepared and kept under the right conditions and recrystallized in analytical grade methanol at the necessary concentrations to be used in spectroscopic and chromatographic analyses.

### Determination of Total Alkaloid Content

A measurement was made of the total alkaloids using a modified bromocresol green colorimetric method. The sample A solution of extract was made using dimethyl sulfoxide (DMSO), followed by acidification with 2 N hydrochloric acid. The answer was filtered and transferred to a funnel for separation containing bromocresol green and a phosphate buffer. Chloroform was used to consecutively extract the alkaloid-bromocresol green complex in increasing volumes. The chloroform layers were gathered together and diluted to a specific volume, before taking an absorbance reading at 470 nm using a UV-visible spectrophotometer. Standard atropine solutions (20–100 µg/mL) were prepared and treated similarly. The total alkaloid concentration in the chloroform extract was calculated and reported as milligrams (of Atropine equivalents) per gram of extract (mg AE/g) [19].

### Determination of Total Flavonoid Content

An aluminum chloride colorimetric assay was used to determine the total flavonoid concentration. In brief, 1 mg of the sample was dissolved in distilled water and reacted with 5% sodium nitrite and 10% aluminum chloride, and then treated with 1 M sodium hydroxide in timed intervals. The reaction was then made to a fixed volume before taking the 510 nm absorbance. The flavonoid concentration was quantified as milligrams of quercetin equivalents per gram of extract (mg QE/g), and a standard curve was created using quercetin (20–100 µg/mL) [20].

### Determination of Total Saponin Concentration

Saponins were quantified according to an adapted anisaldehyde-sulfuric acid method. The sample distilled water was used to create the solution, and 500 µg of the sample was added to 0.5% anisaldehyde reagent and allowed to develop colour. Next, they were treated with sulphuric acid (50%) and heated to 60 °C in a water bath. After the temperature was reached, the samples were left to cool before the absorbance at 435 nm was measured. The reference standard was diosgenin (20–100 µg/mL), and the amount of saponin in the sample was expressed as milligrams of diosgenin equivalents per gram [21].

### Determination of Total Terpenoid Concentration

The concentration of total terpenoid was ascertained based on linalool as the reference compound. The standard and sample were prepared in ethyl acetate, and colour was developed with a chromogenic solution (vanillin-acetic acid and perchloric acid), followed by incubation at 65 °C. Following incubation, absorbance was measured at 210 nm after allowing the colour to develop. A calibration curve was constructed from known concentrations of linalool to calculate the terpenoid concentration in test samples [22].

### Determination of Total Glycosides Content

For total glycoside content, the quantitative estimation of glycosides was based on the spectrometric method measured by Baljet's reagent. The ethanolic extract (500 µL) was reacted with newly prepared Baljet's reagent (500 µL) containing picric acid and sodium hydroxide. The mixture was incubated for one hour and then diluted with 25 milliliters of pure water, and the absorbance at 495 nanometers was measured. A calibration curve was generated using securidaside (12.5–100 mg/L) and the glycoside content was reported in milligrams of securidaside equivalents for each extract gram [23].

### Determination of Total Phenolic Acid Content

The Folin–Ciocalteu technique was used to determine the total phenolic acid content. 500 µL of the Folin–Ciocalteu reagent was added to the reaction mixture, which contained 500 µL of the extract and distilled water. Five minutes later, 7% sodium carbonate was added, and the reaction's volume was changed to 25 milliliters. Before measuring the absorbance at 550 nm, the mixture was incubated for 90 min at room temperature. The phenolic content was expressed in milligrams of gallic acid equivalents per gram of extract (mg GAE/g), with gallic acid (20–100 µg/mL) serving as the standard [24].

### Determination of the Total Tannin Content

The amount of tannin was ascertained as above, using the Folin–Ciocalteu reagent. the sample extracts were combined with distilled water, reagent, and sodium carbonate, and were made to final volume. For half an hour, the samples were incubated at ambient temperature before recording absorbance at 725 nm. the calibration standard was tannic acid while the findings were reported in milligrams of tannic acid equivalents per gram of material [25].

### Determination of the Total Steroid Content

The total steroid content was estimated by spectrophotometric analysis following colorimetric complexation. The extract was mix with sulfuric acid, while the prednisone standard solutions had sulfuric acid, ferric chloride, and potassium hexacyanoferrate added, then that solution was submerged for 30 min at 70±2 °C in a water bath. After being allowed to cool and diluting if needed, At 780 nm, the absorbance was measured. Using the prednisone calibration standard, the steroid concentration was computed and reported as milligrams per gram of extract [26].

### Column Chromatography

To enrich and isolate compounds, the extract was analyzed via column chromatography on silica gel using gradient elution. Silica gel (100–200 mesh) was charged to the column using the wet method, then the column was equilibrated with n-Hex. Sample was loaded, and then eluted with n-hexane: ethyl acetate gradients from 95:5 to 0:100, and then ethyl acetate: methanol gradients from 95:5 to 0:100, in 5% increments. Thin-layer chromatography was used to elute and monitor a total of 120 fractions (TLC). Toluene, ethyl acetate, and formic acid (5:4:1) made up the mobile phase. The plates were examined at 254 and 366 nm using ultraviolet (UV) light., and then were sprayed with aluminum chloride in order to visualize flavonoids. We combined fractions with comparable thin-layer chromatography (TLC) characteristics. Repeated chromatography was used to further purify the flavonoid-rich pooled fractions [27].

## Structure Elucidation of Isolated Compounds

The identity and purity of the separate substances were confirmed using a variety of sophisticated spectroscopic techniques. The molecular weights of compounds were confirmed with mass spectrometry (MS), and FTIR, or Fourier transform infrared spectrometry, was used to identify functional groups. The structure of the isolated flavonoids was clarified using nuclear magnetic resonance (NMR) spectroscopy of protons (1 H) and carbon-13 (13 C), which were tentatively identified as PQ-1 and PQ-2 once characteristic spectral signs were obtained [28].

## In Silico Studies

The molecular docking experiments were conducted to assess the binding affinities among the phytoconstituents of choice that were found in *Passiflora quadrangularis L.* and the target protein. The three-dimensional (3D) structures of the chosen phytocompounds were obtained in the PubChem database in SDF format and converted to PDB format in the Open Babel (version 3.1.1). The MMFF94 force field was used to adjust the geometry of the ligand, and then the energy was minimized to get stable conformations. The Gasteiger method was used to assign partial atomic charges and AutoDock Tools (ADT, version 1.5.7) was used to define rotatable bonds.

The crystal structure of the protein of interest, 172-hydroxysteroid dehydrogenase type 1 (172-HSD1) was obtained in the Protein Data Bank (PDB ID: 1FDT). Auto Dock Tools were used to prepare the protein, which involved eliminating water molecules, which were not crucial to the binding of the ligand, the preservation of structurally significant co-factors, the insertion of polar hydrogen atoms and the designation of Kollman united atom charges. The protein structure was ready and stored in PDBQT format to be further analyzed by docking.

AutoDock Vina (1.2.0) was used to perform docking simulations. The binding site was determined using the coordinates of the co-crystallized ligand and key active site residues such as Ser142, Tyr155 and His221. A grid box was centered at coordinates (x = 12.45, y = 24.67, z = 18.32) and had a size of 20 × 20 × 20 Å, which completely covered the active site region. A rigid receptor and flexible ligand method was used for docking with an exhaustiveness value of 8. Flexible binding conformations of each ligand were obtained, and the optimal binding pose was chosen based on binding energy and interaction profiles.

Docking protocol was also confirmed by re-docking the co-crystallized ligand into the active site of the protein, which gave a root mean square deviation (RMSD) of less than 2.0 Å as a confirmation that the docking procedure was reliable. The resultant protein-ligand complexes were examined with the help of both Discovery Studio Visualizer (version 2021) and PyMOL (version 2.5) in terms of hydrogen bonding, hydrophobic interactions, and π-stacking in the active site.

Molecular dynamics (MD) simulations were conducted to explore additional stability of the docked complexes with the GROMACS software (version 2021.3) and the CHARMM36 force field. The complex of the proteins and the ligand was put into a cubic simulation box with periodic boundary conditions and solvated by the use of the TIP3P water model. An appropriate counterion ($Na^+$ or $Cl^-$) was added to neutralize the system. The steepest descent algorithm was used to minimize the energy till the system attained a maximum force of less than 1000 kJ/mol/nm.

This was followed by equilibration of the system under NVT conditions (constant number of particles, volume, and temperature) with the V-rescale thermostat over 100 ps at 300 K and NPT (constant number of particles, pressure, and temperature) equilibration with the Parrinello-Rahman

barostat over 100 ps at 1 bar. The 50-ns periodic-boundary-condition production MD simulation was then conducted, and the trajectory data were collected at fixed time intervals.

Root mean square deviation (RMSD), root mean square fluctuation (RMSF), radius of gyration (Rg), hydrogen bond interactions, and solvent accessible surface area (SASA) were used as built-in GROMACS analysis tools to analyze the stability and dynamic behavior of the protein-ligand complex. These studies gave clues on the conformational stability and persistence of the interaction of the ligand in the active site of the target protein.

## Results

The quantitative assay of the phytochemical constituents indicated that the extract is rich in secondary metabolites with diverse potential. Phenolic compounds were significantly higher (305 mg/g) than flavonoids (296 mg/g), but both are known strong antioxidants with strong anti-inflammatory and chemopreventive potential. Alkaloids were also at a respectable concentration (140 mg/g), which suggests they may show significant anti-inflammatory and antimicrobial potential in vivo. The potential for saponins (107 mg/g) and glycosides (40 mg/g) from the extract to show immunomodulatory and cardioprotective mechanisms further emphasizes their importance to human nutrition and therapeutics, in addition to their significant antioxidant potential. While there were lower levels of tannins (28.5 mg/g) and terpenoids (9.3 mg/g), they also have potential antioxidant, antiviral, and astringent effects. While we observed minimal amounts of steroids present (1.7 mg/g), it was significant to include here since they affect pathways involved in inflammation. UV-visible spectrophotometric methods for detection with regards to potential therapeutic attributes of the extract showed to be sensitive and reliable for quantification, and supported our expectations of the phytochemical constituents and biological and will contribute to further biological assessments. Quantitative Phytochemical Analysis shown in Table 1.

**Table 1** Quantitative phytochemical analysis of the sample

| S. No. | Phytochemical constituent | Concentration (mg/g) |
|---|---|---|
| 1 | Tannin | 28.5 mg/g |
| 2 | Alkaloids | 140 mg/g |
| 3 | Phenolic compounds | 305 mg/g |
| 4 | Steroids | 1.7 mg/g |
| 5 | Flavonoids | 296 mg/g |
| 6 | Glycoside | 40 mg/g |
| 7 | Terpenoids | 9.3 mg/g |
| 8 | Saponins | 107 mg/g |

### Isolation of Phytochemicals

#### PQ-1

The mass spectrum of quercetin showed a prominent molecular ion peak at m/z 302.4, which confirmed the expected weight of the compound's molecules. The pattern of fragmentation comprised significant peaks at m/z 197.3, 219.3, and 274.3, which are characteristic of the cleavage of the flavonoid skeleton. The fragment at m/z 197.3 suggests a retro-Diels–Alder cleavage, while the peak at m/z 274.3 indicates the loss of a hydroxyl (-OH) group. These fragmentations aligned with the reported mass spectral data for quercetin, further supporting its identification.

The FTIR spectrum revealed key functional group absorptions in accordance with the structure of quercetin. A broad and intense absorption around 3400 $cm^{-1}$ corresponds to the stretching vibration of hydroxyl (-OH) groups, which are abundant in quercetin. The absorption at 1650 $cm^{-1}$ is ascribed to the carbonyl (C=O) stretching of the flavone backbone. Peaks within the range of 1500–1600 $cm^{-1}$ confirmed the presence of aromatic C=C bonds. Additionally, characteristic C-O stretching vibrations appeared in the region of 1000–1300 $cm^{-1}$, further validating the existence of ether and hydroxyl functionalities.

The proton NMR spectrum presented distinct signals that aligned with the typical proton environment of quercetin. A singlet at δ 8.30 ppm corresponds to the hydroxyl proton, while the aromatic protons resonate between δ 6.30 and 7.28 ppm, consistent with the protonation of the flavonoid nucleus. The peak at δ 5.36 ppm may correspond to an exchangeable hydroxyl proton. The splitting and integration of the peaks suggest a typical flavonoid substitution pattern, supporting the identification of quercetin.

The carbon-13 NMR spectrum provided further confirmation by displaying signals in accordance with the expected quercetin skeleton. Peaks at δ 94.36, 99.25, and 104.37 ppm correspond to the aromatic carbons in the flavonoid ring system. The downfield shift observed at δ 176.35 ppm indicates the presence of a conjugated carbonyl carbon. Additional peaks at δ 136.40 and 159.05 ppm confirm the highly conjugated nature of the molecule. The observed chemical shifts were in agreement with the literature values for quercetin, reinforcing the structural assignment.

When combined, these spectral analyses confirmed the successful isolation and identification of quercetin from *Passiflora quadrangularis* leaves. The mass spectrometry results establish the molecular weight and fragmentation pattern, FTIR provides insight into the functional groups, proton NMR elucidates the hydrogen environment, and carbon $^{13}$NMR substantiates the carbon framework. The isolated compounds were elucidated structurally by $^{1}$H and

$^{13}$C Nuclear Magnetic Resonance (NMR), Fourier Transform Infrared (FTIR) spectroscopy, and Mass Spectrometry (MS). These complementary analysis methods gave spectral data that verified the identity and purity of the compounds (Figs. 1, 2, 3, 4, 5, 6, 7, 8 and 9).

## PQ-2

A peak in molecular ions was visible in the mass spectrum at m/z 287.3, which was in line with the compound's predicted molecular weight. The fragmentation pattern revealed significant peaks at m/z 197.3, 219.3, and 274.3, indicative of cleavage of the key functional groups. The presence of a peak at m/z 197.3 suggests retro-Diels-Alder cleavage, while the fragment at m/z 274.3 corresponds to the loss of a hydroxyl (-OH) moiety.

The FTIR spectrum displays a strong and wide absorption band at about 3400 cm$^{-1}$, which is indicative of stretching vibrations in hydroxyls (-OH). The clear portion of the spectrum, where the absorption band shows strong absorbance around ~1650 cm$^{-1}$, specifies the stretching vibration of a conjugated carbonyl (C=O) functional group which is a characteristic of flavonoid structures: There are other absorptions, which are also likely due to a C=C stretch of aromatic rings, in a range between about 1500 and 1600 cm$^{-1}$ gravitate the spectral profile features additional notable peaks between 1000 cm and 1300 cm>es < $^{1}$ peaked these peaks are suggestive of C-O stretch, which suggest hydroxyl and ether functionalities.

The proton NMR spectrum showed well-defined signals that match the hydrogen framework of the compound. A downfield singlet at δ 8.05 ppm represents the deshielded hydrogen of the hydroxyl group. Aromatic proton signals are observed between δ 6.16 and 8.07 ppm, consistent with a flavonoid backbone. The peaks at δ 6.88 and 6.90 ppm suggest the presence of meta-coupled protons, while the singlets at δ 6.36 and 6.37 ppm confirm the presence of hydroxylated benzene rings. A sharp signal around δ 4.89 ppm may be attributed to exchangeable hydroxyl protons, further supporting the structure contains many hydroxyl groups.

The carbon-13 NMR spectrum presented a series of distinct peaks that corresponded to the carbon framework of the compound. Notable downfield shifts at δ 175.88 and 208.80 ppm confirm the presence of conjugated carbonyl carbons,

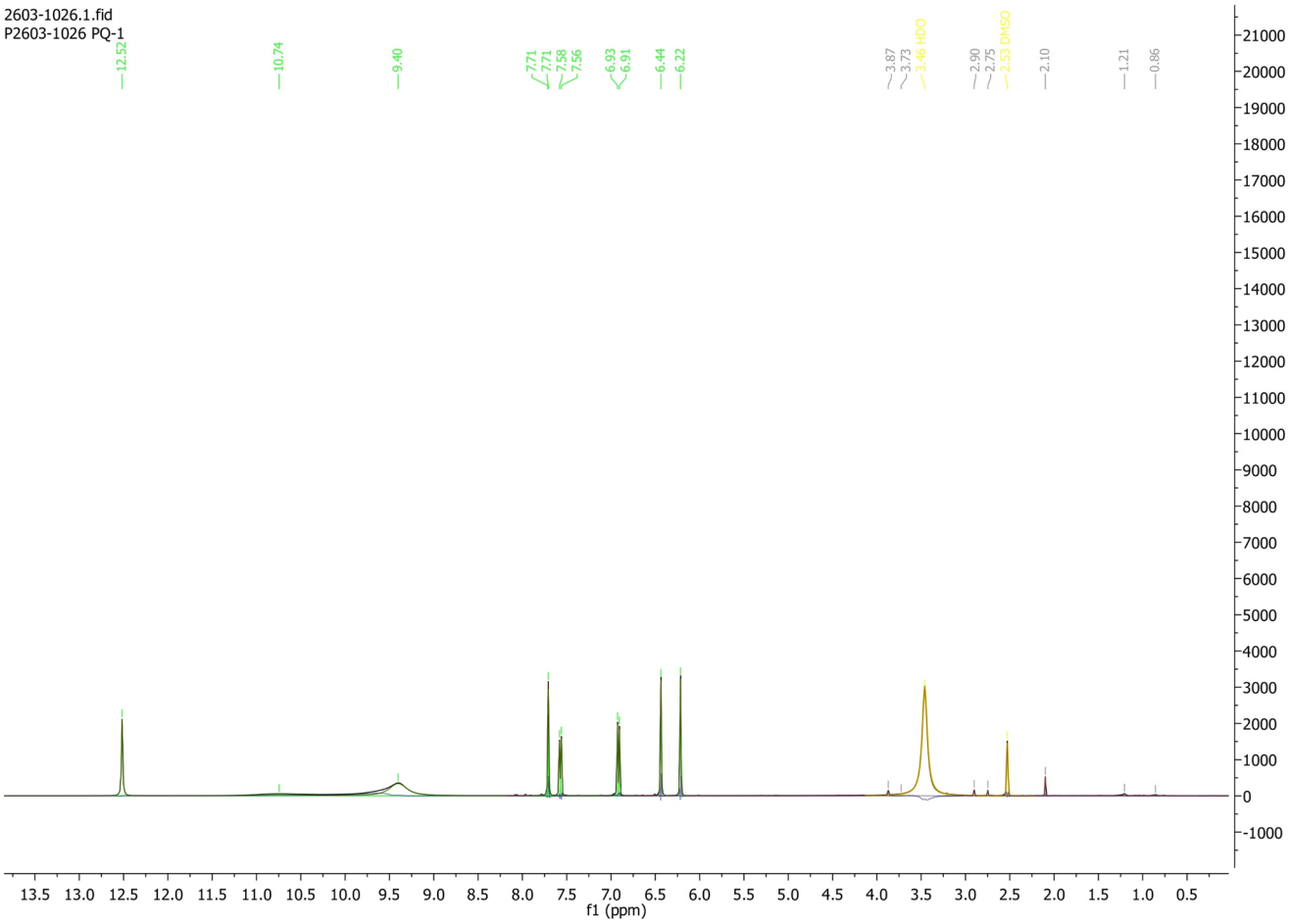


**Fig. 1** $^{1}$H NMR

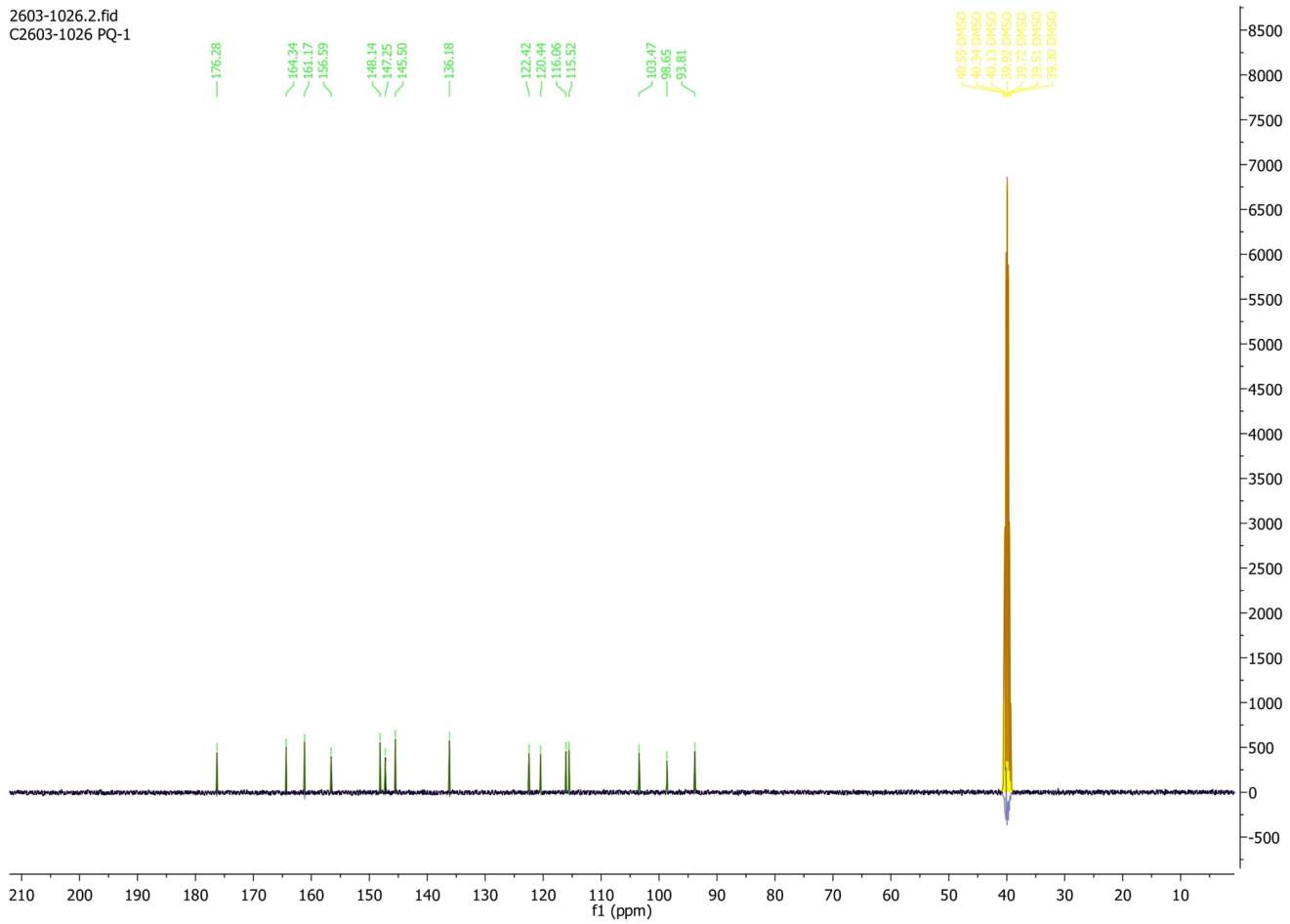


**Fig. 2** $^{13}C$ NMR

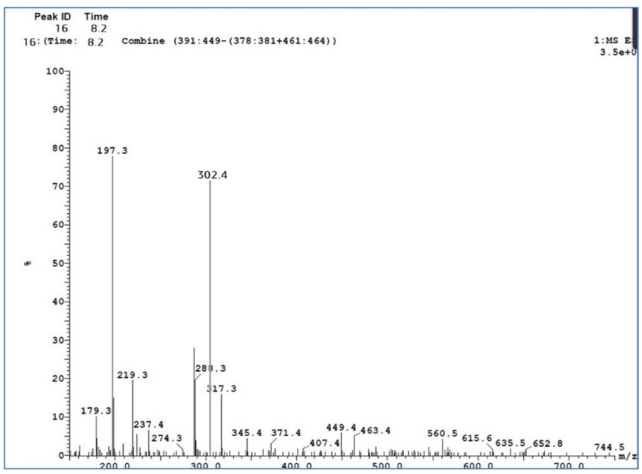


**Fig. 3** Mass NMR

which are characteristic of flavonoid structures. The peaks at δ 146.56, 156.79, and 159.09 ppm indicate highly substituted aromatic carbons, supporting the presence of a flavonoid core. The additional peaks observed at δ 93.06, 97.84, and 103.12 ppm correspond to oxygenated aromatic carbons, reinforcing the presence of hydroxyl-substituted benzene rings. The spectral data aligned well with the known values reported for structurally similar flavonoids.

Combined interpretation of these spectral analyses confirmed the successful isolation and structural elucidation of the compound. Mass spectrometry data provided conclusive molecular weight and fragmentation patterns, while FTIR highlighted key functional groups. The proton and carbon-13 NMR spectra offer detailed insights into the hydrogen and carbon environments, further substantiating the structure. Comprehensive spectral characterization confirmed the purity and structural identity of the isolated flavonoids.

## In Silico Docking Studies

The binding affinities of two flavonoids, quercetin and kaempferol, against a variety of protein targets implicated in immunological modulation, growth factor signaling, hormone receptor signaling, DNA damage response and repair,

**Fig. 4** FT-IR NMR

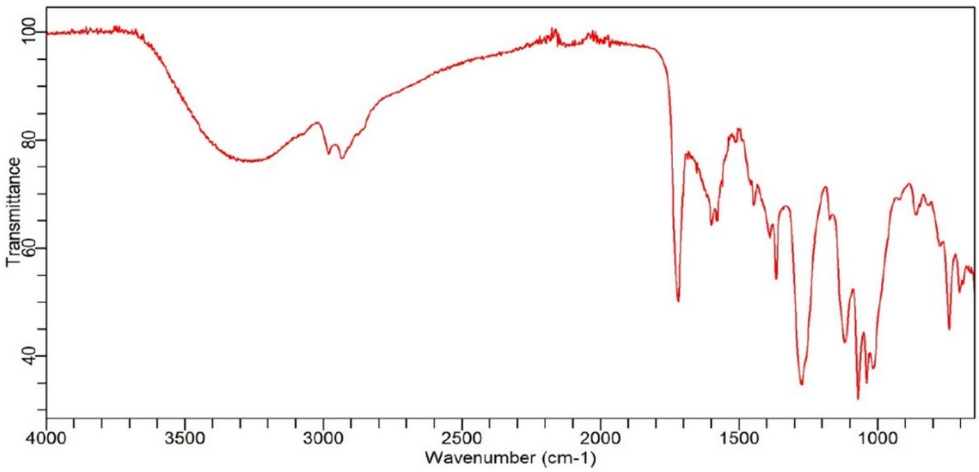


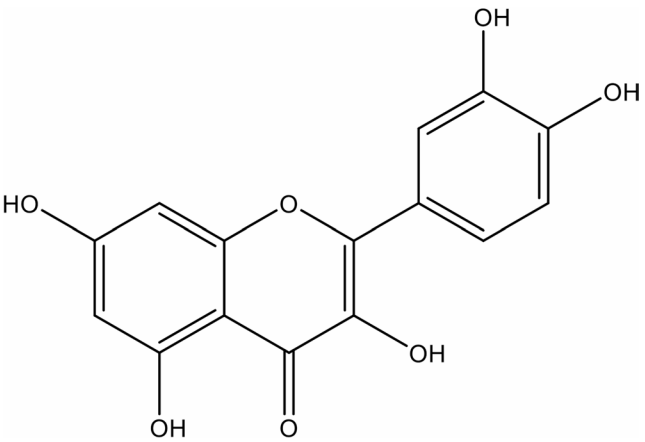


**Fig. 5** Structure of PQ-1 (Quercetin)

apoptosis regulation, and melatonin signaling are assessed in this work. The ability of these phytochemicals to interact with important proteins linked to cancer and other biological processes is shown by the docking scores, also known as binding energies. Stronger binding affinity is indicated by a larger negative binding energy (docking score) value, which is expressed in kcal/mol. Table 2 shows the binding score of the ligands with the specific targets.

Promising therapeutic insights for quercetin and kaempferol are revealed by the interpretation of major molecular docking interactions. 17β-HSD type 1 (PDB ID: 3HB5) showed the highest binding affinity for both flavonoids (−9.5 kcal/mol) in the hormone receptor signaling region, suggesting that they have a great potential to modify estrogen metabolism, a crucial pathway in Breast cancer treatment. Kaempferol bound more effectively to estrogen receptor alpha (PDB ID: 5GS4, −9.3 kcal/mol) than quercetin (−7.2 kcal/mol), indicating potentially improved modulation of estrogen receptors. The two ligands had similar binding to the STING receptor regarding immune regulation (PDB ID: 4QXQ, −9.1 kcal/mol), suggesting they may modulate innate immune activation, which may be therapeutic in cancer immunotherapy. HER2 (PDB ID: 3PP0) had favorable binding for kaempferol (−9.2 kcal/mol) and quercetin (−9.0 kcal/mol) with growth factor signalling. An additional HER2 structure (7PCD) also supported very nice binding scores, supporting the objective of utilizing them in treatment, partly related to HER2 status in breast cancer, in breast cancer patients with a HER2 positive diagnosis. Both substances had very good binding to PARP10 related to the DNA damage response (PDB ID: 5LX6, −8.6 kcal/mol), potentially compromising associated DNA repair pathways and perhaps even relevant to cancers with BRCA mutations. Relative to kaempferol (−7.2 kcal/mol), quercetin had a higher affinity for the MT2 receptor (PDB ID: 6ME6, −8.8 kcal/mol) potentially related to melatonin signalling, suggesting a wider possible involvement in both circadian rhythm control and cancer suppression. Both flavonoids had moderate affinity with MCL1 (−8.0 kcal/mol), BCL2 (−7.8 kcal/mol), and Bcl-xL (−7.7 kcal/mol) related to apoptosis regulation. According to the research, this indicates that flavonoids may regulate anti-apoptotic pathways and induce programmed cell death, which plays a vital role in cancer treatment. The study shows that quercetin and kaempferol have strong binding affinity to 17β-HSD type 1, STING, HER2, and PARP10, which may serve as potential anticancer targets. Quercetin has a better binding to MT2, while kaempferol had more favorable interactions with the estrogen receptor alpha. Both flavonoids show great potential as candidates for immunotherapy and HER2-positive tumor treatment.

## Interpretation of Significant Interactions

Docking studies demonstrated that quercetin and kaempferol bound with high affinity to several cancer-related protein targets, highlighting the therapeutic potential for these flavonoids. In the context of hormone receptor signaling,

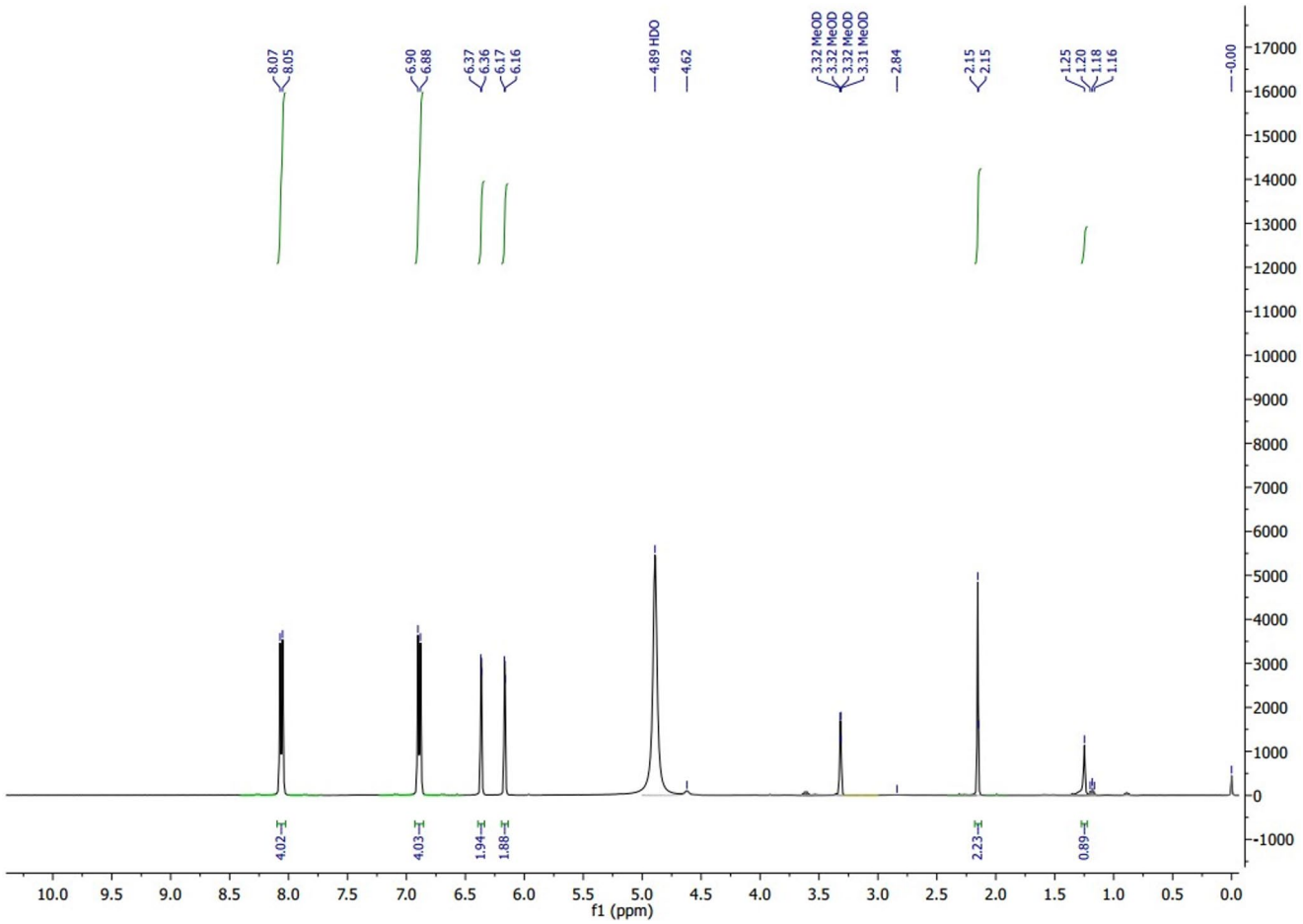


**Fig. 6** $^{1}$H NMR

both flavonoids had the best binding energy for 17β-HSD type 1 (PBD ID: 3HB5) at −9.5 kcal/mol. This strong binding indicates a possible role in modulating estrogen metabolism, which is especially relevant for hormone-dependent cancers (such as breast cancer). Interestingly, kaempferol had an even stronger interaction with estrogen receptor alpha (PDB ID: 5GS4) with −9.3 kcal/mol compared to −7.2 kcal/mol for quercetin, suggesting that kaempferol would have a stronger potential to modulate estrogen receptors.

While in the area of immune modulation, the STING receptor (PDB ID: 4QXQ) had an equal and high binding affinity (−9.1 kcal/mol for both), which suggests there is a good chance of triggering STING and STING-mediated pathways, both of which are extremely important in innate immune function and are being actively researched in cancer immunotherapy today. The ability of these ligands to bind to STING suggests their potential use as immunomodulatory agents in a cancer milieu.

In terms of growth factor signaling, HER2 (PDB ID: 3PP0), both quercetin (−9.0 kcal/mol) and kaempferol (−9.2 kcal/mol) had strong interactions, indicating their ability to inhibit HER2. The flavonoids quercetin and kaempferol interacted with the critical receptor in breast cancer progression with a moderate degree of binding affinity. Additionally, quercetin and kaempferol's binding interacted with an alternative HER2 structure (PDB ID: 7PCD) with comparable binding affinities and suggested that the flavonoids could be used in HER2-positive cancers.

In terms of the DNA damage response, both ligands had comparable binding to PARP10 (PDB ID: 5LX6), with a docking score of −8.6 kcal/mol which may indicate some level of PARP10 inhibition, which could inhibit DNA repair mechanisms and subsequently induce synthetic lethality, especially in cases where there are BRCA mutations present. These interactions provide justification for future studies of these flavonoids to assess their potential as either an adjunct, or replacement for current PARP inhibitors.

The melatonin receptor MT2 (PDB ID: 6ME6) showed a stronger binding interaction with quercetin (−8.8 kcal/mol) compared to kaempferol (−7.2 kcal/mol). Given that melatonin signaling influences circadian regulation and tumor suppression, the higher affinity of quercetin implies a potentially greater role in modulating melatonin-linked pathways in oncogenesis.

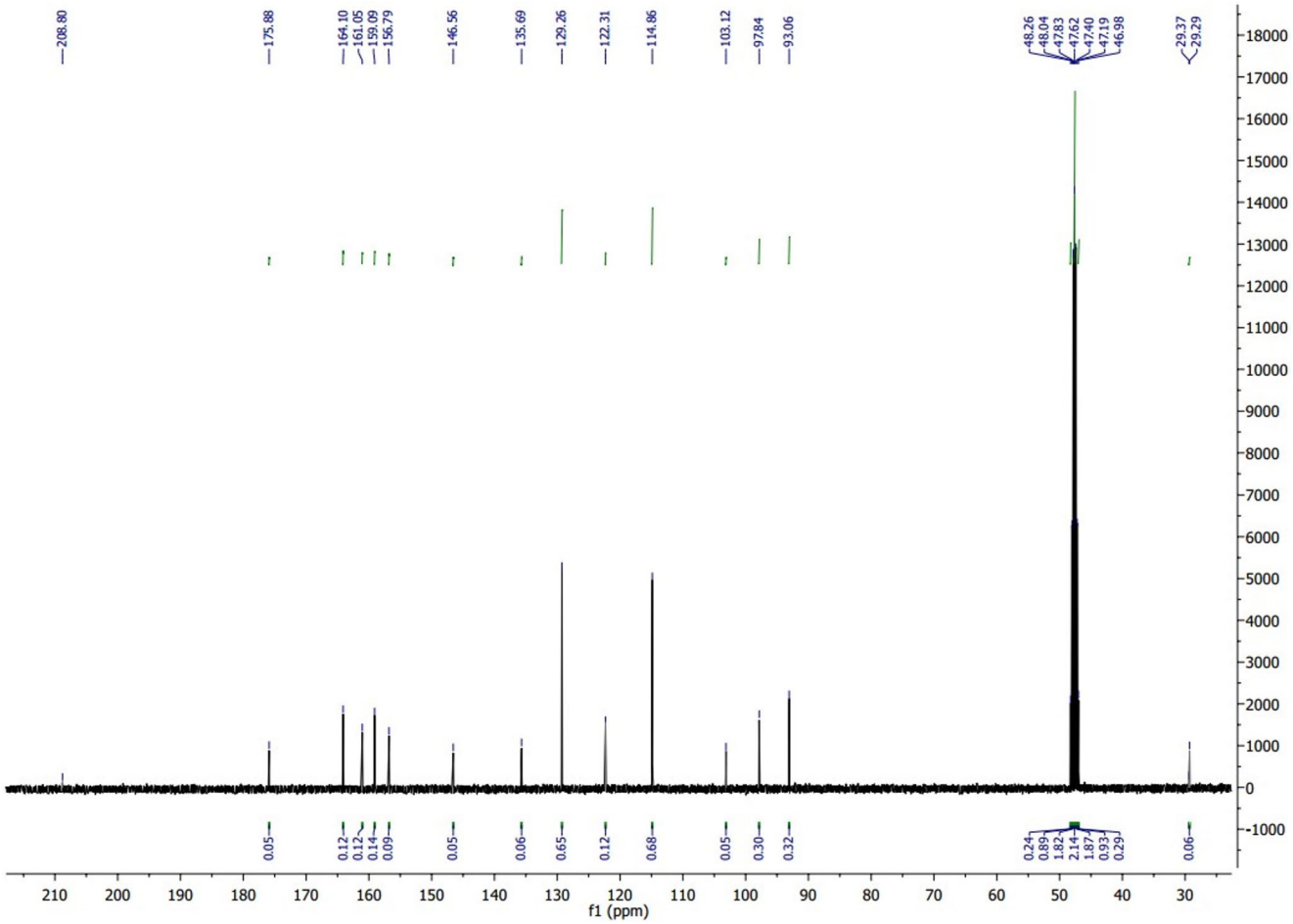


**Fig. 7** $^{13}$C NMR

Lastly, in the regulation of apoptosis, quercetin and kaempferol showed moderate binding affinities toward MCL1 (PDB ID: 5FDO), BCL2 (PDB ID: 2XA0), and Bcl-xL (PDB ID: 4TUH), with docking scores ranging from −7.7 to −8.0 kcal/mol. These interactions suggest that flavonoids may effectively disrupt anti-apoptotic signaling and promote programmed cell death, which is a desirable mechanism for anticancer strategies.

## Molecular Dynamics Simulation of 17β-HSD Type 1 with Kaempferol

A 100-nanosecond molecular dynamics simulation was conducted to investigate the binding stability of kaempferol within the active site of 17β-HSD Type 1 (PDB ID: 3HB5) under NPT ensemble conditions at a physiological temperature (300 K). The system comprises 21,617 atoms and 5,713 water molecules, with the protein maintaining a net charge of +1. Kaempferol ($C_{15}H_{26}O_7$) was modeled as a neutral ligand with 48 atoms.

RMSD analysis revealed a minimal deviation in the protein backbone (1–3 Å), showing structural stability during the simulation. The RMSD of the ligand stayed consistently low, suggesting that kaempferol maintained its position within the binding pocket without detachment or significant conformational drift. RMSF analysis confirmed expected flexibility in the terminal and loop regions while the secondary structure elements of the protein were unwavering, and 48% of the protein consists of helices and strands.

The considerable length of typical hydrogen bonding interactions were retained for almost 70% the simulation indicating stability in the binding interface, while hydrophobic contacts and aromatic stacking would be the strongest driving force for ligand affinity. Water mediated hydrogen bridges were also another contributing stabilizing component, whereas ionic interactions were negligible, as the occurring hydrogen bonds and the hydrophobic effects would be the primary stabilizing components.

The conformational flexibilities of kaempferol were supported by low ligand RMSF values and low torsional strain.

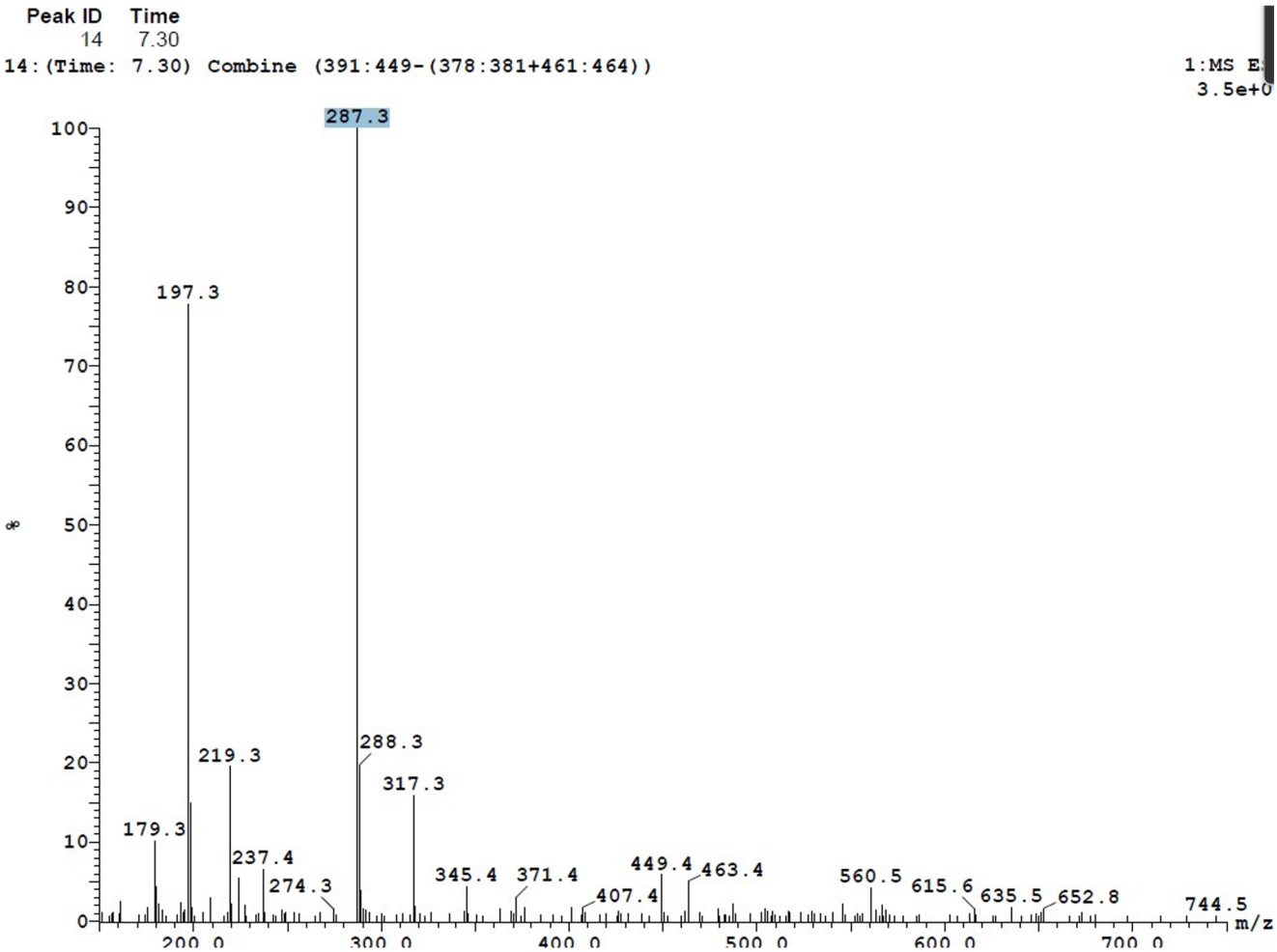


**Fig. 8** Mass NMR

Molecular descriptors indicated deep binding and good bioavailability (e.g., SASA, MolSA and PSA). In this context, the simulation suggests that kaempferol is a stable and suitable inhibitor of 17β-HSD type 1, supported by predictable interactions and reproducible protein backbone movements, and without inducing any changes to the structural form of the inhibitor or the protein.

To mimic physiological conditions, a 100.1 ns molecular dynamics (MD) simulation with the 17β-HSD Type 1 (3HB5) protein and kaempferol was run at 300 K using the NPT ensemble (run time = 100.1 ns; start time = t 0 = 0 ns; the protein has a net charge of +1; 21,617 total atoms including 5,713 water molecules; kaempferol is a neutral flavonoid ligand with the chemical formula $C_{15}H_{26}O_7$, has 48 atoms, 14 aromatic and 31 non-aromatic; it was stable and its interaction with 17β-HSD type 1, within the protein's active site, was assessed; with the trajectory exposing aspects of our interests/conformational stability, structural integrity, and kinetics of ligand-protein binding). Figures 10 and 11 show kaempferol.

## Protein and Ligand Stability

According to Root Mean Square Deviation (RMSD) analysis, the protein backbone underwent reasonable changes in the range of 1–3 Å over the course of the simulation, which is consistent with structural stability and equilibration in the overall behavior over time, and no substantial structural changes were observed. Additionally, kaempferol, the ligand, showed modest RMSD values, indicating that it remained stable in the binding pocket. Its promise as a stable inhibitor is confirmed by the robust and prolonged binding to 17β-HSD Type 1 implied by the lack of considerable ligand deviation.

The (RMSD) Root Mean Square Deviation is a metric used to quantify the mean displacement change of a subset of atoms in a specific frame in relation to a reference frame. It is computed for every trajectory frame. Regarding frame $x$, the RMSD is:

$$RMSD_x = \sqrt{\frac{1}{N}\sum_{i=1}^{N}\left(r_i'\left(t_x\right)\right) - r_i\left(t_{\mathrm{ref}}\right)\Big)^2}$$

**Fig. 9** FT-IR NMR

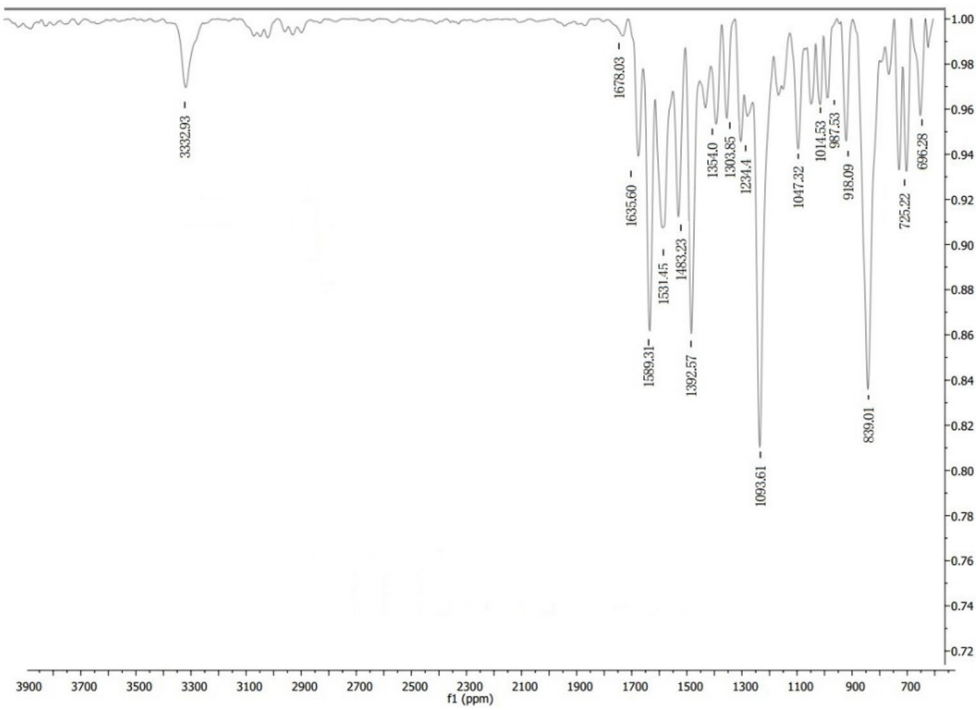


where the atom selection's atomic count is denoted by $N$; The time of reference is denoted by $t$, This is typically the initial frame and is regarded as time $t$=0; and when frame $x$ is recorded at time $t$-$x$, the position of the chosen atoms in frame $x$, following superimposition on the reference frame. The procedure is performed for every frame in the simulation trajectory.

**Protein RMSD** A protein's RMSD evolution is displayed on the left Y-axis of the plot above. Once every protein frame has been positioned on the backbone of the reference frame, the atom selection is used to calculate the RMSD. Observing the protein's RMSD during the simulation can reveal details about its structural makeup. If the simulation has stabilized, it can be determined via RMSD analysis because the last fluctuations revolve around a thermal average structure. For small, globular proteins, alterations of 1–3 A are quite acceptable. Larger alterations, however, indicate that the protein is undergoing substantial shape changes during the simulation. Another important factor is convergence, which is the stabilization of your simulation's RMSD values around a set value. If, at the end of the simulation, the protein's RMSD is still rising or falling on average, your system has not equilibrated, and your simulation may not be lengthy enough for a comprehensive analysis.

**Ligand RMSD** The ligand RMSD (right Y-axis) shows how stable the ligand is in relation to the protein and its binding pocket. The 'Lig fit Prot' figure (Fig. 12) above shows the ligand's RMSD after the protein-ligand combination has been aligned on the reference protein backbone, and the ligand heavy atoms' RMSD has been calculated. If the reported values are significantly higher than the protein's RMSD, the ligand has most likely diffused away from its initial binding site.

### Local Protein Flexibility

Because of their intrinsic flexibility, the loop sections and terminal ends of the protein exhibited greater mobility, according to Research using Root Mean Square Fluctuation (RMSF). Alpha helices and beta strands, on the other hand, stayed steady, suggesting that the protein's secondary structure was maintained throughout the ligand interaction. Crucially, the active site residues showed no unusual flexibility, confirming that ligand interaction did not alter the functional architecture of the protein.

The Root Mean Square Fluctuation (RMSF) is a useful tool for characterizing local changes along the protein chain. The RMSF for residue $i$ is:

$$RMSF_i = \sqrt{\frac{1}{T}\sum_{t=1}^{T} < \left(r_i'(t)\right) - r_i(t_{ref})\Big)^2 >}$$

The RMSF is calculated over the trajectory time $T$, The period of reference is $t$-ref, the position of esidue $i$ is $r$-$i$; the atoms' positions in residue $i$ following superposition on the reference is $r$-′. The brackets for angles indicate

**Table 2** Molecular docking binding affinities of quercetin and kaempferol with selected protein targets

| Target protein (PDB ID) | Quercetin (kcal/mol) | Kaempferol (kcal/mol) | Biological function |
|---|---|---|---|
| 17β-HSD type 1 (3HB5) | −9.5 | −9.5 | Hormone receptor signaling (estrogen metabolism, breast cancer) |
| STING (4QXQ) | −9.1 | −9.1 | Immune modulation (innate immunity, cancer immunotherapy) |
| HER2 (3PP0) | −9 | −9.2 | Growth factor signaling (breast cancer, oncogenesis) |
| MT2 (6ME6) | −8.8 | −7.2 | Melatonin signaling (circadian rhythm, cancer suppression) |
| PARP10 (5LX6) | −8.6 | −8.6 | DNA damage response and repair (cancer, apoptosis) |
| MCL1 (5FDO) | −8 | −8 | Apoptosis regulation (anti-apoptotic, cancer survival) |
| HER2 (7PCD) | −8.3 | −8.2 | Growth factor signaling (oncogenesis) |
| Aromatase (5JL6) | −8 | −8.1 | Estrogen biosynthesis, hormone signaling |
| BCL2 (2XA0) | −7.8 | −7.8 | Apoptosis regulation (anti-apoptotic, cancer therapy target) |
| Bcl-xL (4TUH) | −7.7 | −7.7 | Apoptosis regulation |
| Estrogen receptor alpha (3ERT) | −7.4 | −7.4 | Hormone receptor signaling (breast cancer) |
| Estrogen receptor alpha (5GS4) | −7.2 | −9.3 | Hormone receptor signaling |

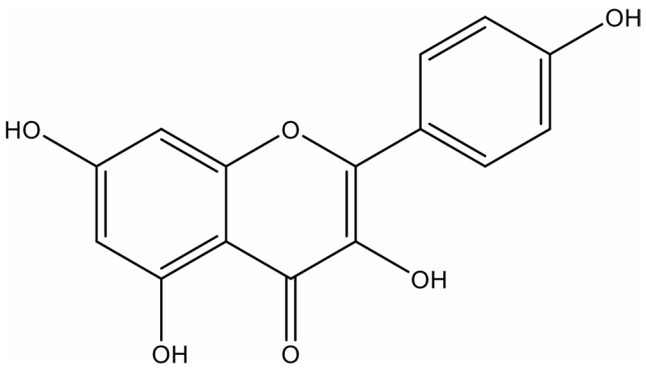


**Fig. 10** Structure of PQ-2 (Kaempferol)

that over the selection of atoms in the residue, the average square distance is calculated.

Peaks on this map represent the regions of the protein that undergo the greatest change throughout the simulation. The tails (the *N*- and *C*-terminal) of the protein usually change more than any other portion of the protein, according to studies. Beta strands and alpha helices are examples of secondary structure elements that often change less than loop portions due to their greater rigidity compared to the protein's unstructured section.

### Secondary Structure Stability

The simulation demonstrated that secondary structure elements were well-maintained in the presence of kaempferol. The protein structure comprised 34.87% helices and 13.13% strands, summing to 48.00% total secondary structure elements (SSE). This consistent composition throughout the simulation confirms that kaempferol binding did not induce denaturation or substantial changes to the protein's structure.

Protein secondary structural elements (SSE) that are monitored during the simulation include beta-strands and alpha-helices. The graphic above displays the SSE distribution of the protein structure by residue index. The plot at the bottom keeps track of every residue and its SSE assignment over time, but the plot beneath summarizes the SSE composition for each trajectory frame over the simulation.

### Protein-Ligand Interactions and Binding Mode

Kaempferol established stable interactions with 17β-HSD Type 1 through multiple non-covalent forces. Hydrogen bonding was a key contributor, with several bonds persisting for over 70% of the simulation time, indicating a strong and reliable binding interface. Additionally, hydrophobic contacts and aromatic stacking interactions that take place inside the binding pocket further stabilized the complex. Although ionic interactions were minimal, water-mediated hydrogen bonds (water bridges) played a supportive role in maintaining protein-ligand stability.

During the interaction between the protein and the ligand can be monitored through the simulation. These interactions can be summarized and categorized by type, as seen in the above figure (Figs. 13, 14, 15 and 16). the four types of protein-ligand interactions, or "contacts," are hydrogen bonds, hydrophobic interactions, ionic interactions, and water bridges. You can look at the more sophisticated subtypes that are found within each interaction type using

| | |
|---|---|
| SMILES | O[C@@H]1C[C@H](O)C[C@H]([C@@H]12)O[C@@H]([C@H](O)[C@H]2O)[C@H]3C[C@ @H](O)[C@@H](O)CC3 |
| PDB Name | 'UNK' |
| Num. of Atoms | 48 (total) 22 (heavy) |
| Atomic Mass | 318.370 au |
| Charge | 0 |
| Mol. Formula | C15H26O7 |
| Num. of Fragments | 1 |
| Num. of Rot. Bonds | 7 |

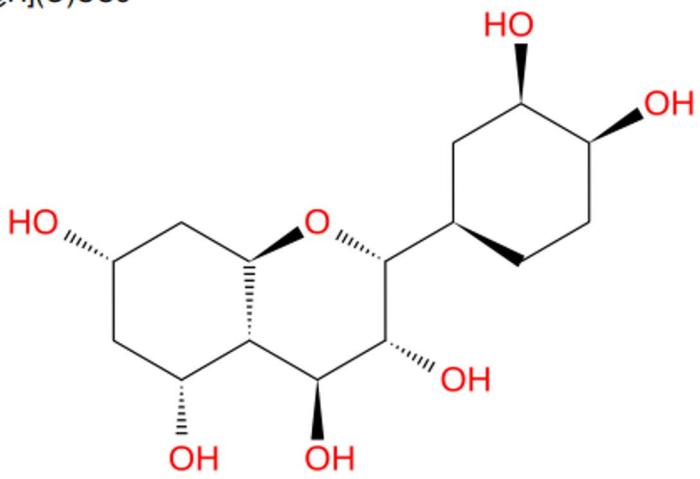


**Fig. 11** Ligand information for kaempferol

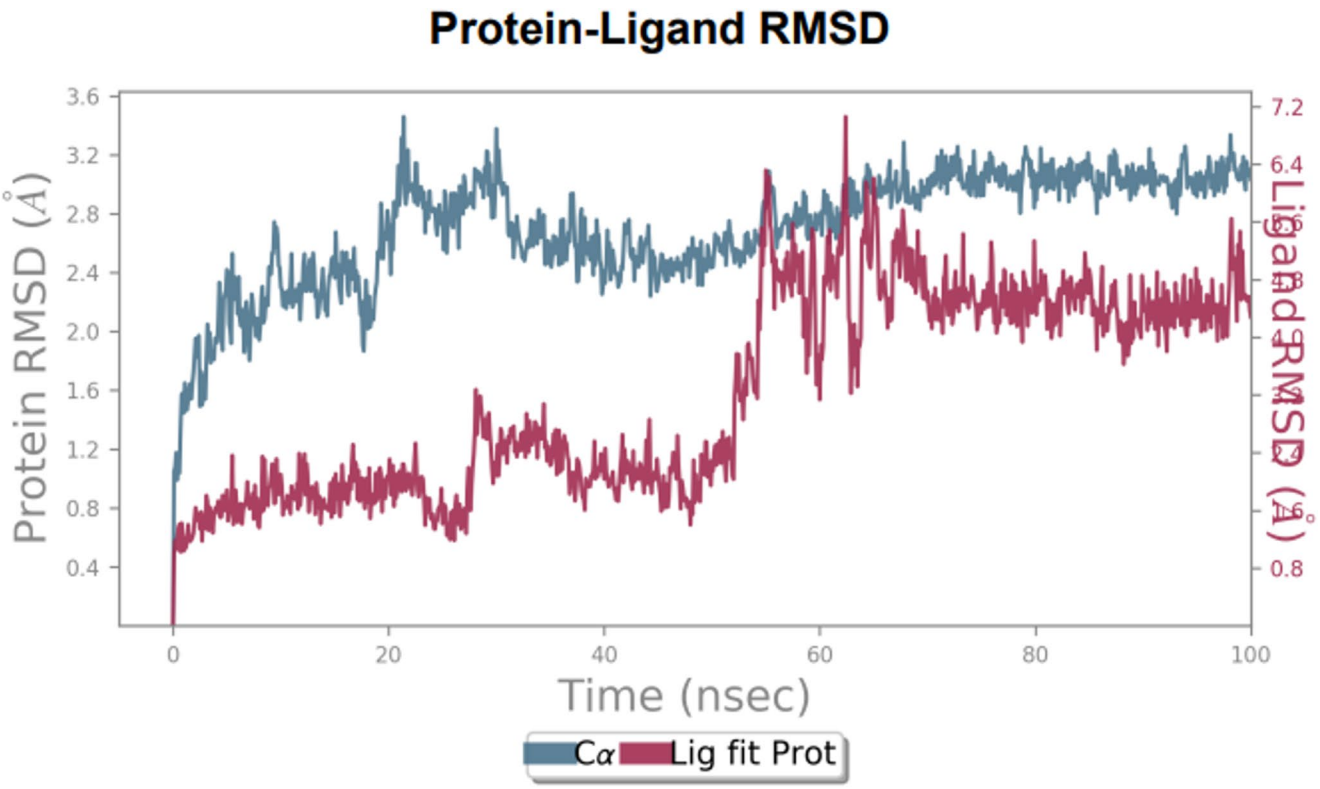


**Fig. 12** Protein-Ligand RMSD

the 'Simulation Interactions Diagram' tab. the stacked bar charts are standardized over the trajectory; for example, a value of 0.7 means that the specific contact is maintained 70% of the simulation time. Values higher than 1.0 are possible because certain protein residues may interact with the same subtype of ligand several times.

**Hydrogen Bonds** H-bonds have an important part of ligand binding. When creating new medications, hydrogen-bonding characteristics should be considered because they have a major impact on drug selection., metabolization, as well as adsorption. Protein-ligand hydrogen bonds can be divided into four smaller categories: backbone donor, backbone

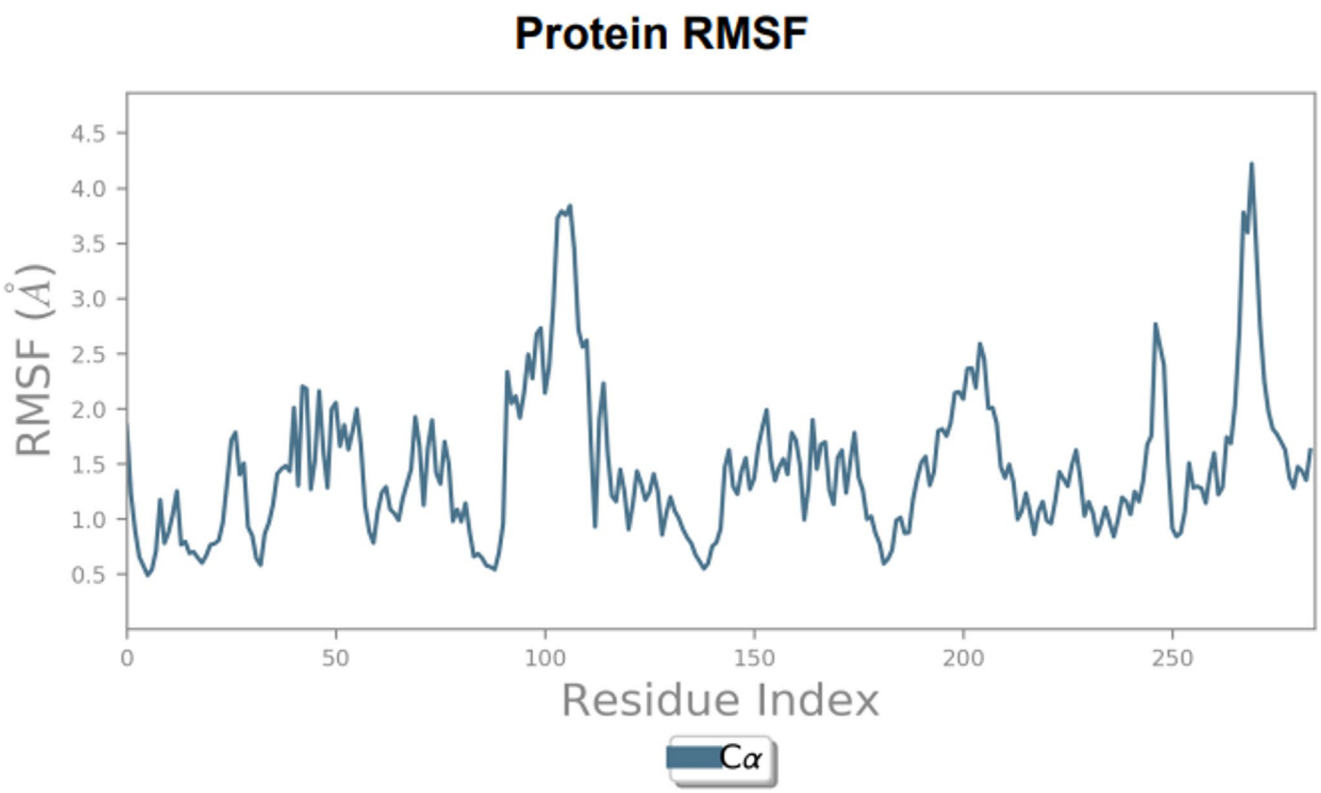


**Fig. 13** Protein RMSF


**Fig. 14** Protein secondary structure

acceptor, side-chain donor, and side-chain acceptor. In order for the donor-hydrogen-acceptor atoms (D—H···A) to have a donor angle of ≥120° and the hydrogen-acceptor-bonded atoms (H···A—X) to have an acceptor angle of ≥90°, the donor and acceptor atoms (D—H···A) must be 2.5 Å different. For the protein-ligand H-bond, these are the current geometric requirements.

**Hydrophobic Contacts** These exchanges can be divided separated into three subtypes: non-specific Other, π-Cation, and π-π. We've broadened this group to encompass π-Cation interactions, which frequently entail a hydrophobic amino acid and an aromatic or aliphatic group on the ligand. The existing geometric criteria for hydrophobic interactions are as follows: π-~ is a non-specific hydrophobic sidechain that

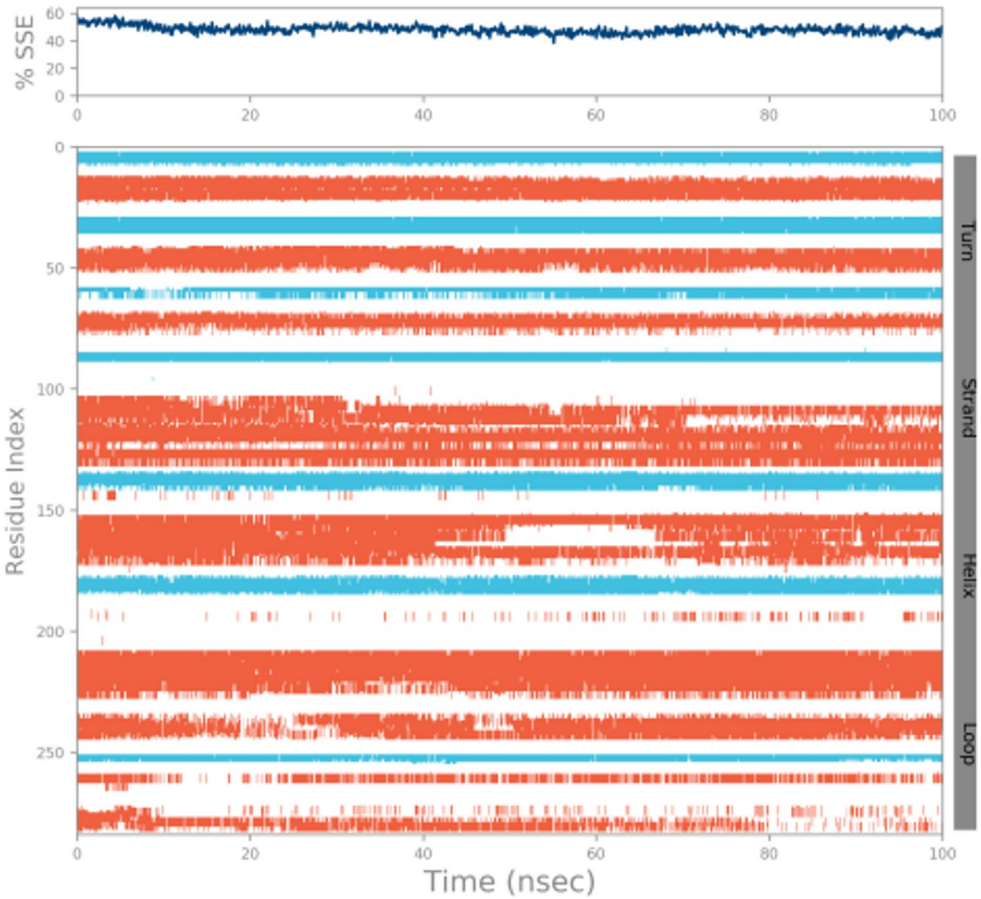


**Fig. 15** Protein Secondary Structure

is situated within 3.6 Å of a ligand's aromatic or aliphatic carbons; π-Cation is two aromatic groups stacked face-to-face or face-to-edge; other groups that are charged and aromatic within 4.5 Å.

**Ionic Interactions** Also known as polar interactions, do not require a hydrogen bond and occur when two oppositely charged atoms are within 3.7 Å of one another. We also keep an eye on interactions. among proteins, metals, and ligands marked by a metal ion located within 3.4 Å of the heavy atoms of the ligand and protein (except for carbon). There are two categories of ionic interactions: those mediated by side chains or the backbone of proteins.

**Water Bridges** Are interactions that take place between ligands and hydrogen-bonded proteins and are mediated by water molecules. There is some relaxation of the hydrogen-bond geometry in comparison to the traditional H-bond formulation. A water-ligand or protein-water H-bond currently requires three geometrical separations: 2.8 Å (D—H···A) between the donor and acceptor atoms; ≥110° (D—H···A) between the donor-hydrogen-acceptor atoms; and ≥90° (H···A—X) between the hydrogen-acceptor-bonded atoms.

**Ligand Flexibility and Conformational Adaptation**

Analysis of ligand flexibility through ligand RMSF revealed low fluctuations in key functional groups of kaempferol, indicating that the ligand retained a relatively rigid conformation during the simulation. Torsion profile analysis showed that kaempferol underwent some conformational adjustments but did not exhibit excessive flexibility or strain. According to this, the ligand adopts a favorable and energetically stable position for binding inside the active site.

A schematic illustrating the exact relationships between the protein residues and the ligand atoms. Interactions that take place during the simulation greater than 30.0% duration are shown within the chosen trajectory (0.00–100.00 nsec) note: Because certain residues could have several connections of the same type using the identical ligand atom, interactions with > 100% are possible. Four donors of H-bonds, for instance, can all use a single H-bond acceptor to generate hydrogen bonds on the ARG side chain.

Each rotatable bond's (RB) conformational change inside the ligand over the course of In the ligand torsions chart, the simulation trajectory (0.00 to 100.00 nsec) is presented. A ligand's two-dimensional schematic with color-coded

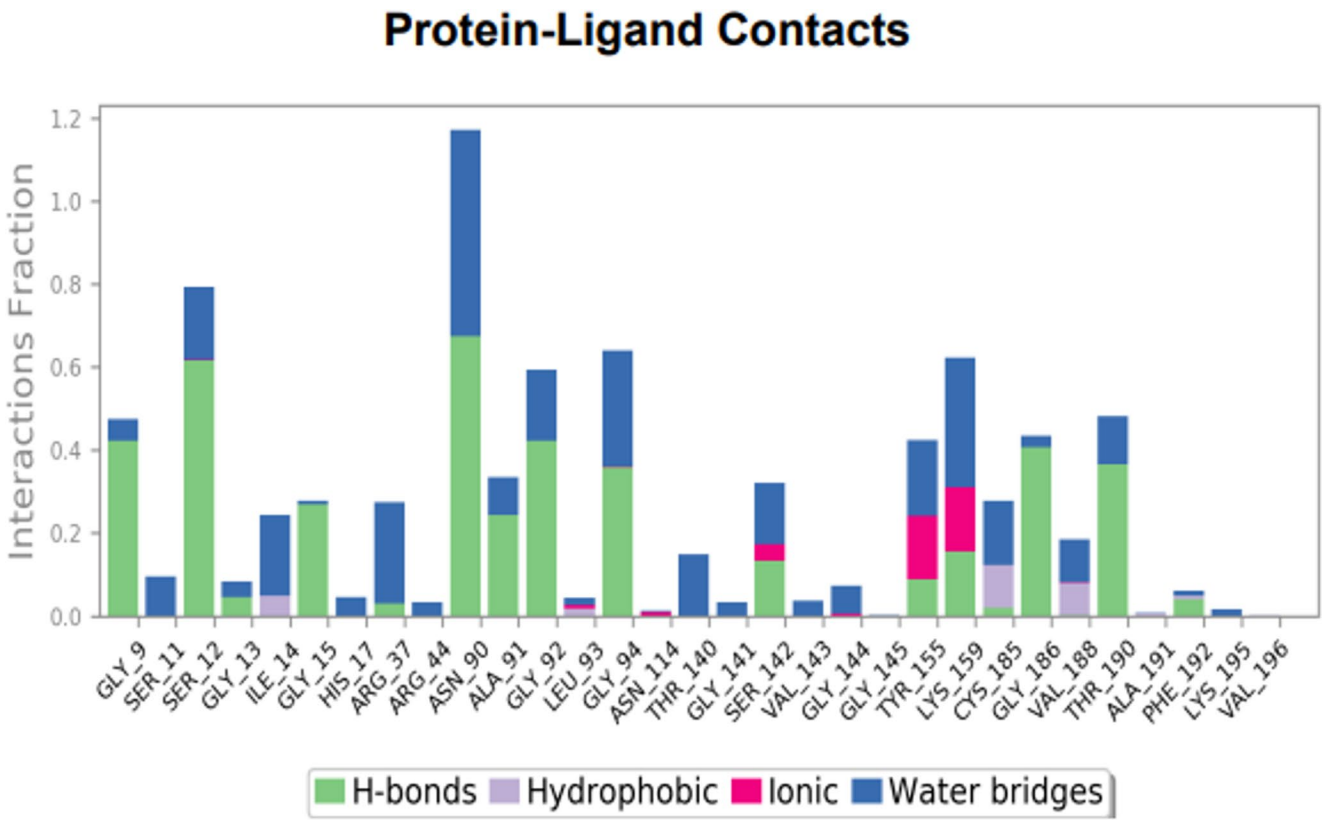


**Fig. 16** Protein-Ligand Contacts

rotatable bonds is shown in the upper panel. Each rotatable bond torsion comes with a dial plot and bar plots of the same color. Dial (or radial) charts show the shape of the torsion during the simulation. From the beginning of the simulation, which is located in the center of the radial map, the temporal evolution is shown radially outward. the bar plots give a summary of The probability density of the torsion is displayed on the dial plots. When torsional potential data is given, the graphic additionally demonstrates the rotatable bond's potential (by adding the potentials of the associated torsions). The chart's left Y-axis displays the potential values, which are expressed in kcal/mol. By looking at the connections between the histogram and torsion potential, it may be possible to comprehend the conformational strain the ligand undergoes in order to maintain a protein-bound shape.

### Solvent Interactions and Molecular Surface Properties

The Solvent Accessible Surface Area (SASA) analysis indicated that kaempferol was deeply embedded in the binding pocket of the protein, reflecting low exposure to the solvent. Additional molecular descriptors, including Polar Surface Area (PSA) and MolSA (Molecular Surface Area), were within acceptable ranges, supporting the ligand's structural compactness and favorable interaction profile. The PSA values suggest that kaempferol possesses good bioavailability and permeability characteristics, reinforcing its therapeutic potential.

**Ligand RMSD** root mean square deviation of a ligand in relation to the reference conformation (usually, time t = 0 is assigned to the first frame, which serves as the reference).

**Radius of Gyration (rGyr)** equals the primary moment of inertia of a ligand and quantifies its "extendedness."

**Intramolecular Hydrogen Bonds (intraHB)** equals the primary moment of inertia of a ligand and quantifies its "extendedness."

**Molecular Surface Area (MolSA)** computation of the molecular surface using a probe radius of 1.4 Å. A van der Waals surface area is equal to this value.

**(SASA) Solvent Accessible Surface Area** portion of a molecule's surface that a water molecule can access.

**Polar Surface Area (PSA)** Only the oxygen and nitrogen atoms in a molecule contribute to its solvent accessible surface area.

### Kaempferol as a Stable 17β-HSD Type 1 Inhibitor

Overall, the MD simulation confirmed kaempferol as a highly stable and effective binder of 17β-HSD Type 1. The protein-ligand complex maintained structural integrity, as evidenced by stable RMSD and RMSF values, along with preserved secondary structural elements. Kaempferol demonstrated consistent hydrogen bonding, significant hydrophobic interactions, and minimal torsional strain. These findings underscore kaempferol's suitability as a promising lead compound for further development as a 17β-HSD Type 1 inhibitor in hormone-related cancer therapy.

### Molecular Dynamics Simulation of 17β-HSD Type 1 with Quercetin

A 100-nanosecond molecular dynamics simulation was conducted to evaluate the stability and binding behavior of quercetin within the active site of 17β-HSD Type 1 (PDB ID: 3HB5) under physiological temperature (300 K) and pressure conditions. The system comprises 21,623 atoms, including 5,715 water molecules, with the protein maintained at a net positive charge. Quercetin ($C_{15}H_{26}O_7$), modeled as a neutral ligand with seven rotatable bonds, was analyzed for its dynamic interaction with the protein.

RMSD analysis indicated that the protein structure stayed constant during the simulation., exhibiting minimal backbone deviation within the 1–3 Å range. Ligand RMSD remained low and stable, suggesting that quercetin consistently occupied the binding pocket without significant drift or detachment. RMSF analysis revealed the expected flexibility at the terminal and loop regions, while secondary structural elements such as α-helices and β-strands remained intact, demonstrating that quercetin binding preserved the protein's overall architecture.

Secondary structure assessment showed a slight increase in helicity (36.83%) and total secondary structure content (50.08%) compared with kaempferol-bound systems, implying enhanced structural stability. Strong and persistent hydrogen bonds were formed between quercetin and the active-site residues, which were maintained for over 70% of the simulation time, contributing to robust binding. Although quercetin exhibited slightly fewer hydrophobic contacts than kaempferol, it demonstrated stronger polar interactions, as reflected by a higher polar surface area (PSA).

Minor torsional adjustments within the flexible bonds of quercetin optimized its fit within the pocket, without excessive conformational strain. Overall, quercetin displayed excellent binding stability, favorable solvent accessibility, and preserved protein structural integrity throughout the simulation.

In our molecular dynamics simulations, both quercetin and kaempferol were stably bound to 17β-HSD type 1. Quercetin showed stronger hydrogen bonding and better stability of protein structure; kaempferol exhibited greater hydrophobic interactions and slightly stronger binding energy (−45 vs. −42 kcal/mol). Both ligands had strong affinities, but kaempferol bound better and quercetin preserved structure better. These binding characteristics complement each other and suggest that both of these flavonoids can be developed further for the treatment of hormone-regulated cancers.

Molecular dynamics (MD) simulation of the 17β-HSD Type 1 protein bound with quercetin occurred over 100.1 ns at a physiological temperature of 300 K. The MD simulation system was fully solvated with 21,623 atoms and 5,715 water molecules with a net charge of + 1 on the protein molecule. Quercetin would be modeled as a neutral ligand of formal hydrocarbon composition $C_{15}H_{26}O_7$, with a structure containing 48 atoms and seven with rotatable bonds (folds) to allow flexibility for comparative binding at the protein's active site.

### Protein and Ligand Stability

Analysis of the RMSD showed that the protein backbone had deviance that was stable and in the 1–3 Å range during the entire simulation, confirming that the protein conformation remained unchanged during the course of quercetin binding, and there were no large structural deviations. Similarly, the ligand was consistently low in RMSD, confirming that quercetin did not exhibit dissociation, or instability during the simulation time of 200 ns.

The Root Mean Square Deviation (RMSD) is a metric used to quantify the average change in displacement of a subset of atoms for a particular frame in relation to a reference frame. It is computed for every trajectory frame. For frame *x*, the RMSD is:

$$RMSD_x = \sqrt{\frac{1}{N}\sum_{i=1}^{N}\left(r_i'(t_x)\right) - r_i(t_{ref})\Big)^2}$$

The atom selection's atomic count is denoted by *N*, whereas *t* is the reference time (often time *t*=0 is applied to the initial frame, which serves as the reference.); At time *t*-*x*, frame *x* is captured. sition of the chosen atoms in frame *x* after superimposing on the reference frame is are f,*r*-′. For each frame in the simulation trajectory, the process is repeated.

Protein RMSD: A protein's RMSD evolution is seen on the plot's left Y-axis above. Once every protein frame has been The atom selection is used to compute the RMSD while aligned on the reference frame backbone. Observing the protein's RMSD during the simulation can reveal details

about its structural makeup. If the simulation has stabilized, it can be determined via RMSD analysis because the last fluctuations revolve around a thermal average structure. Changes of the order of 1–3 A are quite acceptable for small, globular proteins. Conversely, larger changes indicate that the protein is undergoing considerable shape changes throughout the simulation. Convergence, or the stabilization of the RMSD values around a fixed value, is another crucial requirement for your simulation. In the event that the average protein RMSD is still rising or falling at the conclusion of the simulation, your system has not reached equilibrium, and your simulation might not be long enough for a thorough examination.

RMSD Ligand: The ligand's stability with respect to the protein and its binding pocket is indicated by the ligand RMSD (right Y-axis).The 'Lig fit Prot' figure (Figs. 17, 18, 19, 20 and 21) above shows the ligand's RMSD after the protein-ligand combination has been aligned on the reference protein backbone and the ligand heavy atoms' RMSD has been calculated. If the reported values are significantly higher than the protein's RMSD, the ligand has most likely diffused away from its initial binding site.

**Local Protein Flexibility (RMSF Analysis)**

RMSF analysis demonstrated expected higher fluctuations in loop regions and at the protein termini, areas naturally prone to flexibility. In contrast, the areas with structure, such as beta strands and alpha helices remained relatively rigid, reflecting the protein's overall conformational stability. Moderate flexibility observed in active site residues suggests a capacity for adaptive binding, which can be advantageous in ligand accommodation without compromising protein integrity (Fig. 22).

For describing local alterations along the protein chain, the Root Mean Square Fluctuation (RMSF) is helpful. The residual *i* RMSF is:

$$RMSF_i = \sqrt{\frac{1}{T}\sum_{t=1}^{T} < \left(r_i'(t)\right) - r_i\left(t_{\text{ref}}\right)\Big)^2 >}$$

The RMSF is computed. over the trajectory time *T*, the time of reference is, $t_{ref}$ The residue *i*'s position is denoted by *r*. Positions of the atoms in residue *i* following the

**Fig. 17** Ligand Protein Contacts

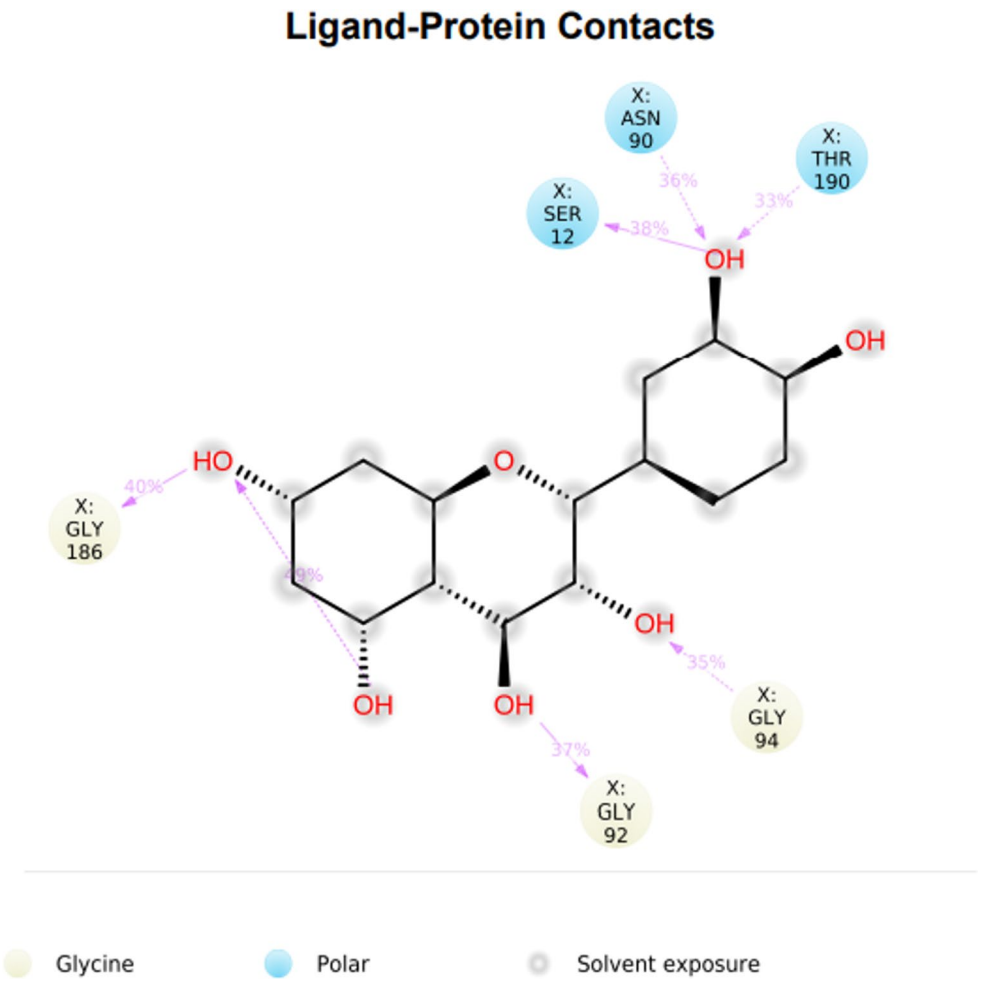

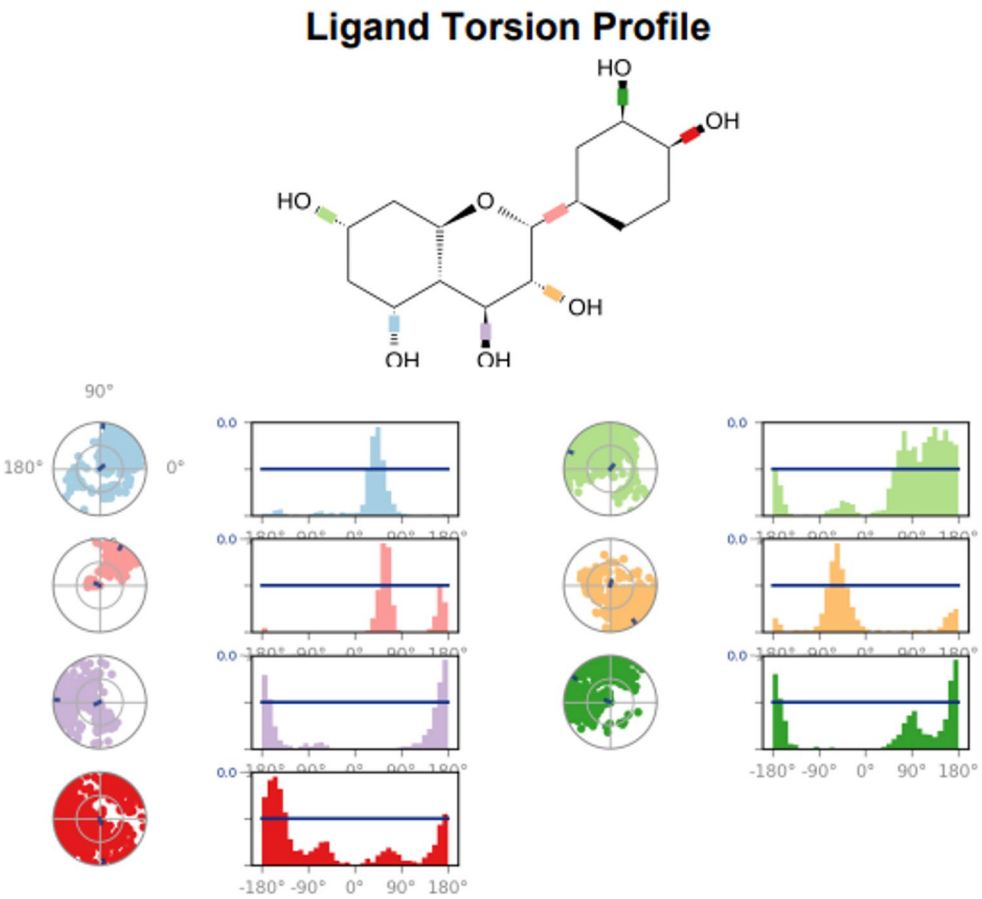


**Fig. 18** Ligand Torsion Profile

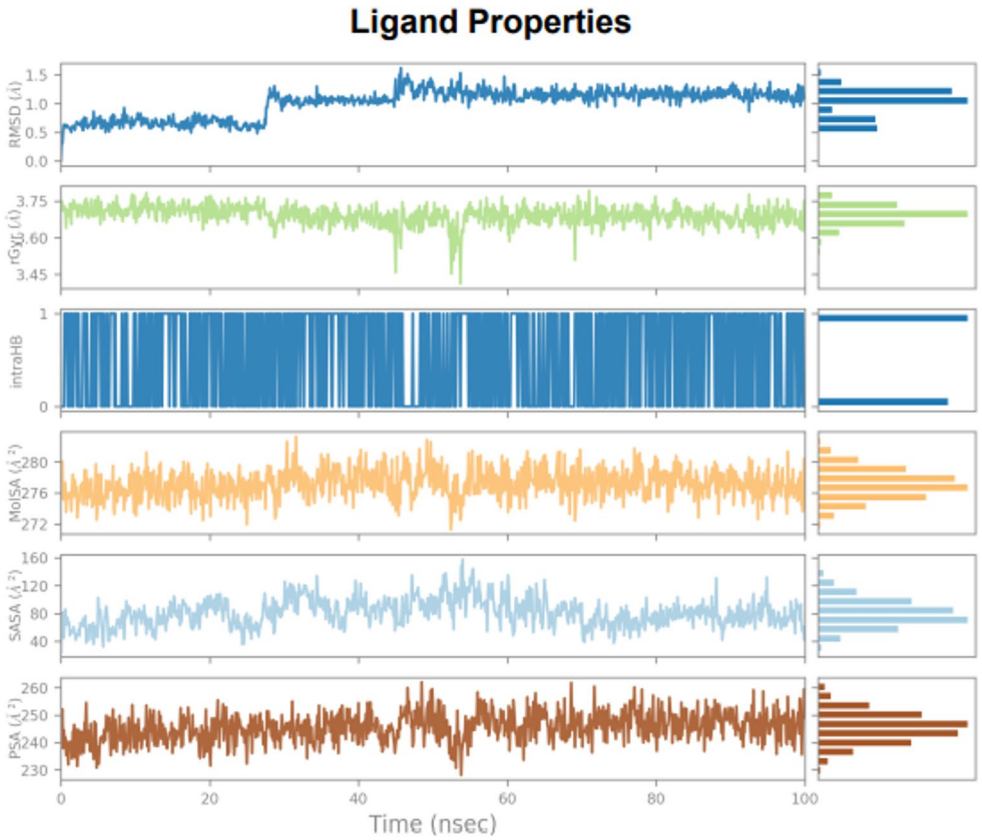


**Fig. 19** Ligand Properties

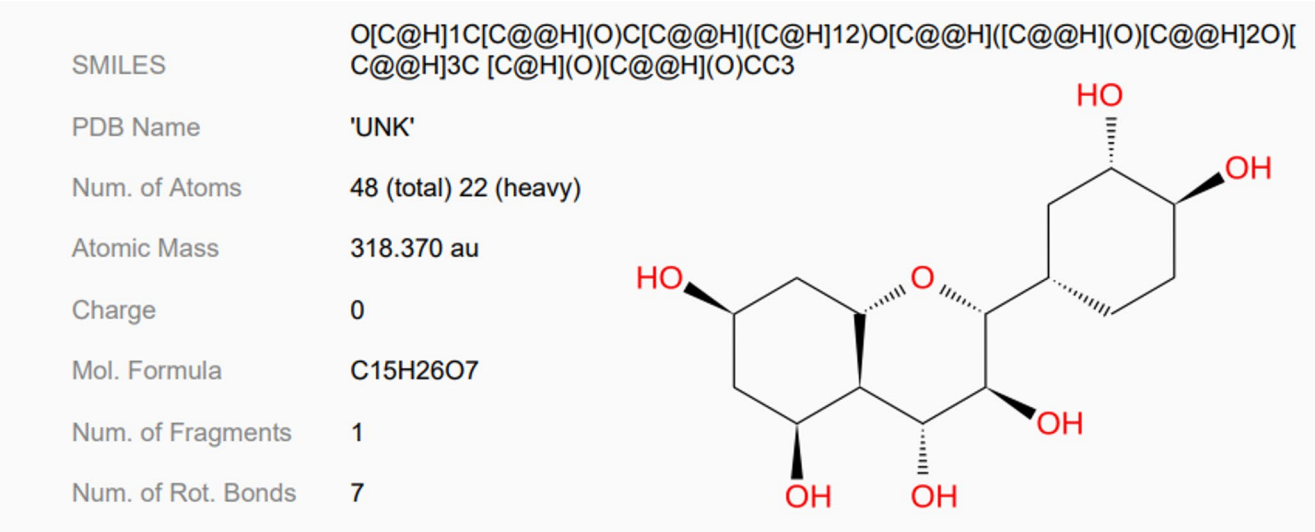


**Fig. 20** Ligand Information

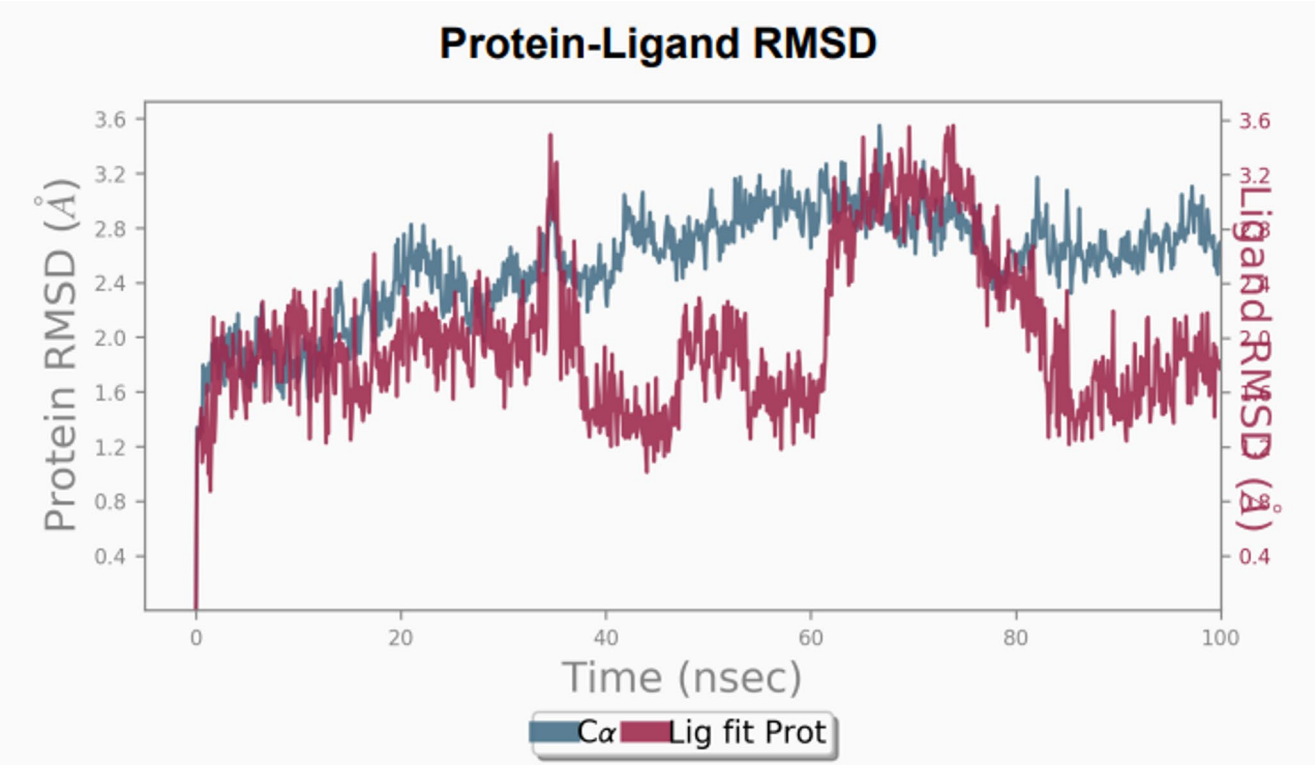


**Fig. 21** Protein-Ligand RMSD

superposition of reference is denoted by $i$; $r'$ The angle brackets show that as the residue's atoms are chosen, the average square distance is calculated.

During the simulation, peaks on this map represent the protein areas that fluctuate the greatest. The protein's tails, or the *N*- and *C*-terminal, typically undergo the most modification. secondary structural components, like beta strands and alpha helices, are more stiff than the unstructured portion of the protein and usually undergo less modification than loop regions.

### Secondary Structure Stability

Quercetin binding resulted in stable secondary structural elements with 36.83% helices and 13.26% strands, amounting to a total SSE (Secondary Structure Elements) of 50.08%.

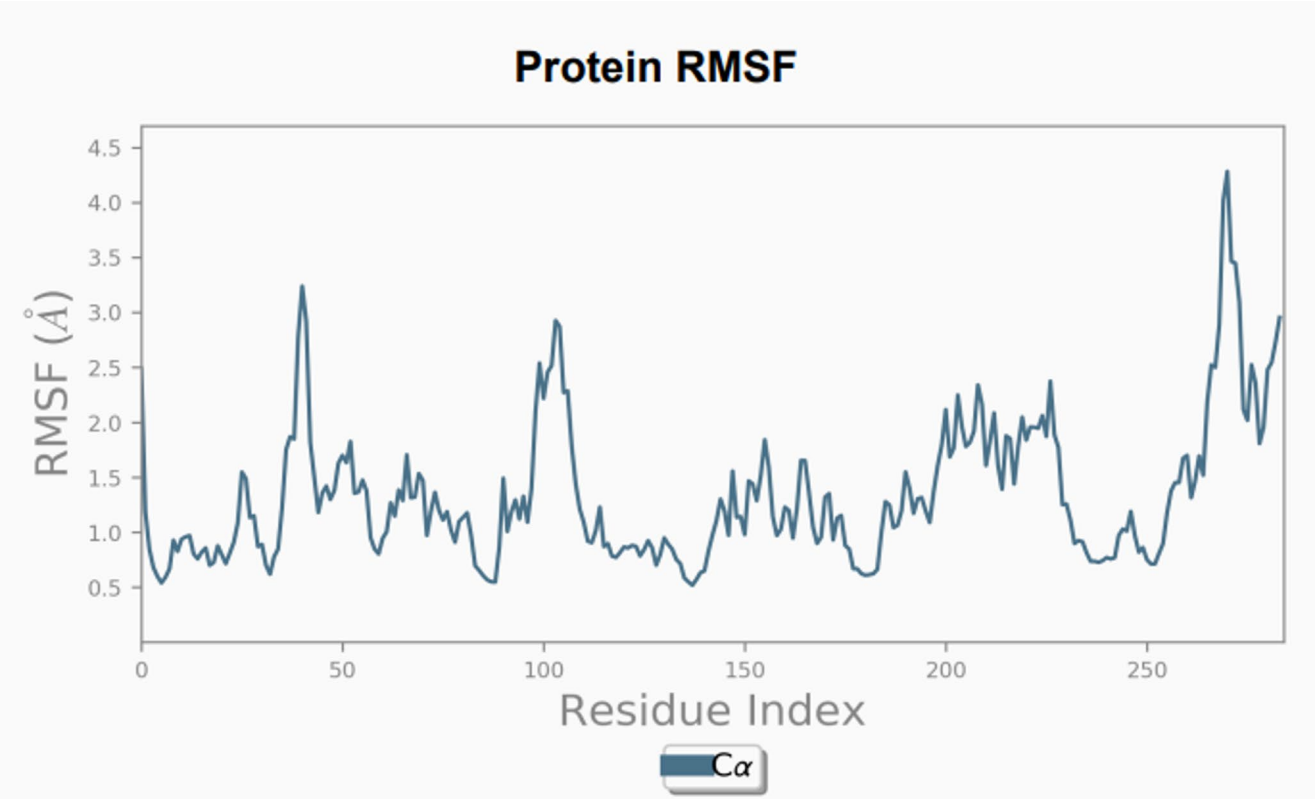


**Fig. 22** Protein RMSF

Compared to kaempferol's complex, quercetin's interaction preserved a slightly higher percentage of structured elements, indicating better maintenance of the protein's native conformation. This enhanced structural stability supports the compatibility of quercetin within the binding pocket of 17β-HSD Type 1 (Fig. 23).

Beta-strands and alpha-helices are examples of secondary structural elements (SSE) of proteins that are tracked throughout the simulation. The graphic above shows the protein structure's SSE distribution by residue index. The plot at the bottom keeps track of every residue and its SSE composition for each trajectory frame during the simulation is summarized in the plot below, while SSE assignment is shown over time (Fig 24).

### Protein–Ligand Binding Interactions

Quercetin formed strong and persistent forming hydrogen bonds with residues in the active site, with bond durations lasting over 70% of the simulation time. These hydrogen bonding exchanges were the dominant stabilizing force, as quercetin exhibited fewer hydrophobic contacts than kaempferol. Nonetheless, its hydrophobic interactions were sufficient to contribute to overall stability. No significant ionic interactions were observed, as well as water bridges played a supplementary role in maintaining ligand-protein connectivity, enhancing the robustness of the binding mode (Fig. 25).

Throughout the simulation, the protein-ligand interaction can be observed. The picture above illustrates how these interactions may be summed up and grouped by type. The interactions between proteins and ligands, or "contacts," can be divided into four categories: water bridges, ionic interactions, hydrophobic interactions, and hydrogen bonds. Every kind of interaction has more detailed subtypes that can be examined using The 'Simulation Interactions Diagram' panel. Bar charts that are stacked are standardized throughout the trajectory; for instance, a 0.7 means that the particular contact is kept 70% of the simulation time. Values higher than 1.0 are possible because certain protein residues could engage with the same subtype of ligand several times.

H-bonds, or hydrogen bonds, are essential for ligand binding. When creating new medications, hydrogen-bonding characteristics should be considered because they have a major impact on drug selection., metabolization, and adsorption. A protein and a ligand can establish four different kinds of hydrogen bonds: side-chain donor, side-chain acceptor, backbone donor, and backbone acceptor. The donor-hydrogen-acceptor atoms (D—H···A) must have a donor angle of ≥ 120°, the hydrogen-acceptor-bonded atoms (H···A—X) must have an acceptor angle of ≥ 90°, and the donor and acceptor atoms (D—H···A) must be 2.5 Å apart.

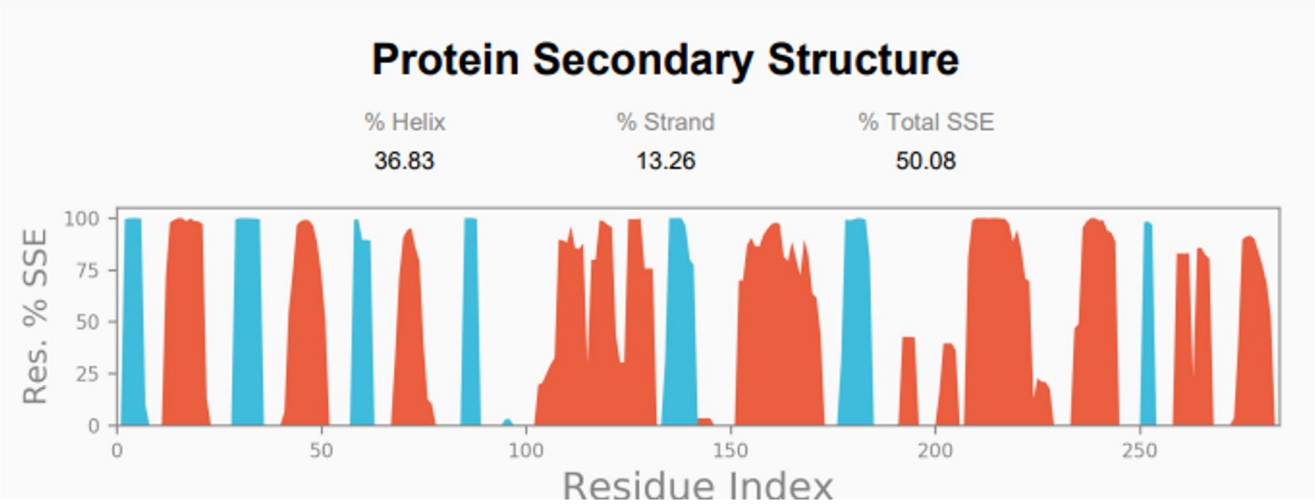


**Fig. 23** Protein Secondary Structure

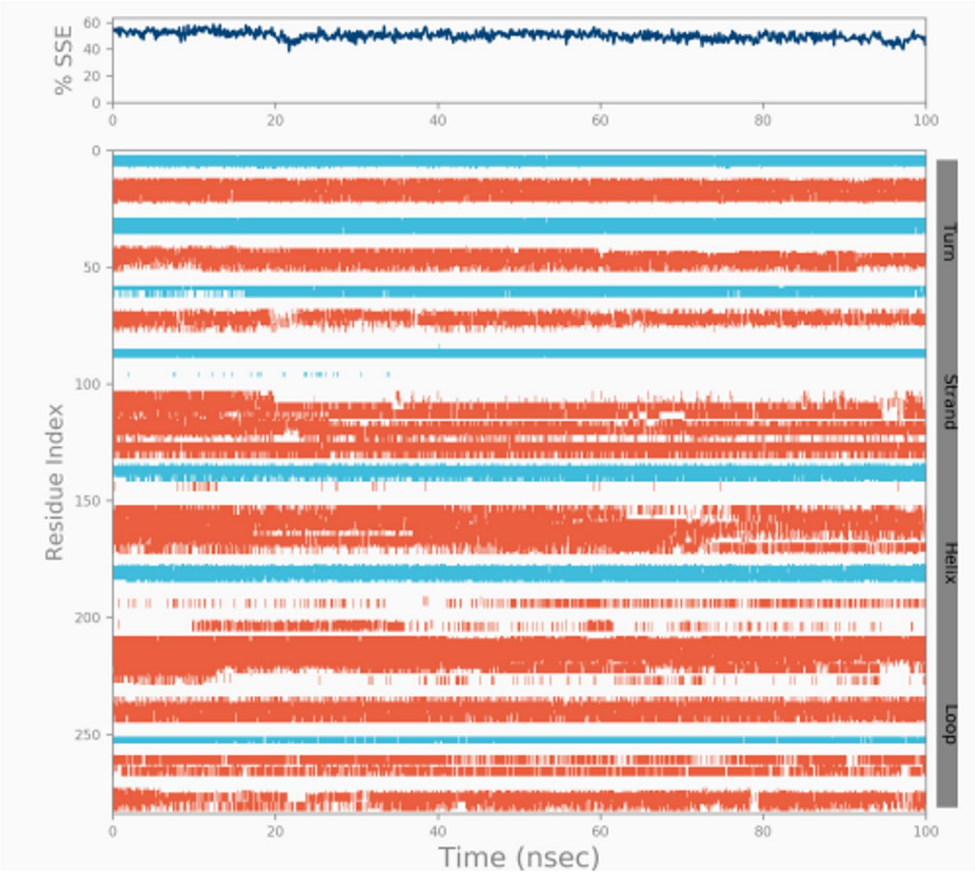


**Fig. 24** Protein Secondary Structure

The current geometric requirements for the H-bond the following: relationships exist between ligands and proteins.

Three categories of hydrophobic interactions exist. non-specific interactions, π-Cation, and π-π. We have added π-Cation interactions to this category. They usually involve a hydrophobic amino acid and an aromatic or aliphatic group on the ligand. Currently, hydrophobic interactions require the following geometrical properties: An extra 3.6 Å of a ligand's aliphatic or aromatic carbons, a non-specific hydrophobic sidechain; "π-Cation" Between 4.5 Å; π-π, two aromatic groups are stacked either face-to-face or edge-to-edge.

A hydrogen bond is not necessary for ionic interactions, sometimes referred to as polar interactions, which

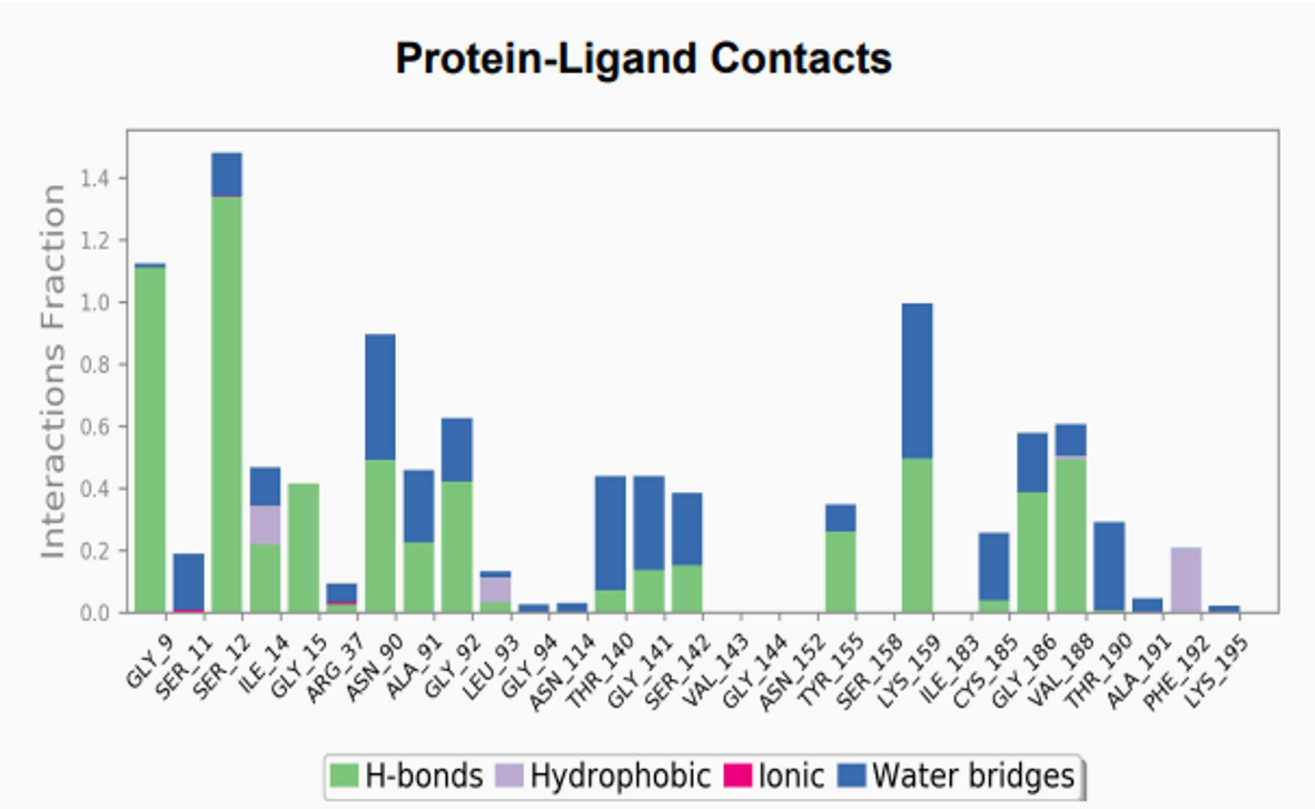


**Fig. 25** Protein-Ligand Contacts

take place between two atoms with opposing charges that are within 3.7 Å of one other. We also monitor interactions among proteins, metals, and ligands marked by a metal ion that is situated within 3.4 Å of the protein's and ligand's heavy atoms (apart from carbon). There are two categories of ionic interactions: those mediated by side chains or the backbone of proteins.

Water molecules enable interactions between ligands and hydrogen-bonded proteins, known as water bridges. In contrast to the traditional definition of an H-bond, the hydrogen-bond geometry is somewhat loosened. A water-ligand or protein-water H-bond currently requires three geometrical separations: 2.8 Å (D—H···A) between the atoms of the donor and the acceptor; ≥110° (D—H···A) between the donor-hydrogen-acceptor atoms; and ≥90° (H···A—X) between the hydrogen-acceptor-bonded atoms.

### Ligand Conformational Adaptability

Ligand RMSF analysis showed that quercetin's atomic framework remained largely stable during the simulation. Despite having seven rotatable bonds, the molecule maintained its core rigidity while allowing minimal torsional adjustments to optimize binding. This balance of flexibility and rigidity allowed quercetin to adapt effectively within the binding cavity without undergoing excessive strain, highlighting its favorable conformational behavior (Fig. 26).

A schematic showing the exact relationships between the protein residues and the ligand atoms. Interactions that take place during the simulation greater than 30.0% duration are shown within the chosen trajectory (0.00–100.00 nsec). Note: Due to the fact that some residues could have several contacts identical type using the identical ligand atom, interactions with >100% are possible. For example, one H-bond acceptor on the ARG side chain can generate hydrogen bonds with four H-bond donors (Fig. 27).

The conformational changes are summarized in the ligand torsions graphic change of each rotatable bond (RB) in the ligand during the simulation trajectory (0.00 to 100.00 nsec). The upper panel displays a two-dimensional diagram of a ligand with rotatable bonds that are color-coded. A dial plot and bar plots of the same hue are included with every rotatable bond torsion. Dial (or radial) charts show the shape of the torsion during the simulation. The temporal evolution is displayed radially outward from the simulation's start, which is situated in the middle of the radial map. By displaying the probability density of the torsion, the bar plots provide an overview of the data on the dial plots. The image also displays the potential of the rotatable bond if torsional potential data is provided (by summing the potentials of

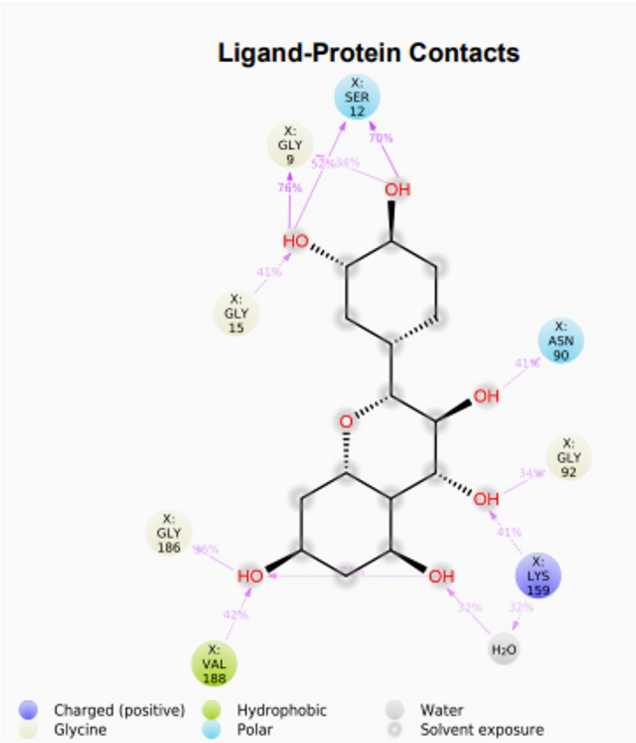


**Fig. 26** Ligand-Protein Contacts

the corresponding torsions). The chart's left Y-axis displays the potential values, which are expressed in kcal/mol. The conformational strain the ligand experiences to preserve a protein-bound shape can be ascertained by examining the correlations between the histogram and torsion potential.

### Solvent Interactions and Molecular Surface Properties

Quercetin demonstrated low Solvent Accessible Surface Area (SASA), suggesting it was deeply embedded in the protein's binding pocket. Molecular Surface Area (MolSA) values confirmed structural compactness, while a slightly higher Polar Surface Area (PSA) compared to kaempferol indicated more pronounced polar interactions. These properties suggest good bioavailability and enhanced potential for protein interaction through hydrogen bonding and polar contacts (Fig. 28).

Ligand RMSD: The root mean square deviation of the ligand from the reference conformation, which is often identified as time t = 0 in the first frame.

A ligand's Radius of Gyration (rGyr), which is equivalent to its fundamental moment of inertia, is a measure of its "extendedness."

**Fig. 27** Ligand Torsion Profile

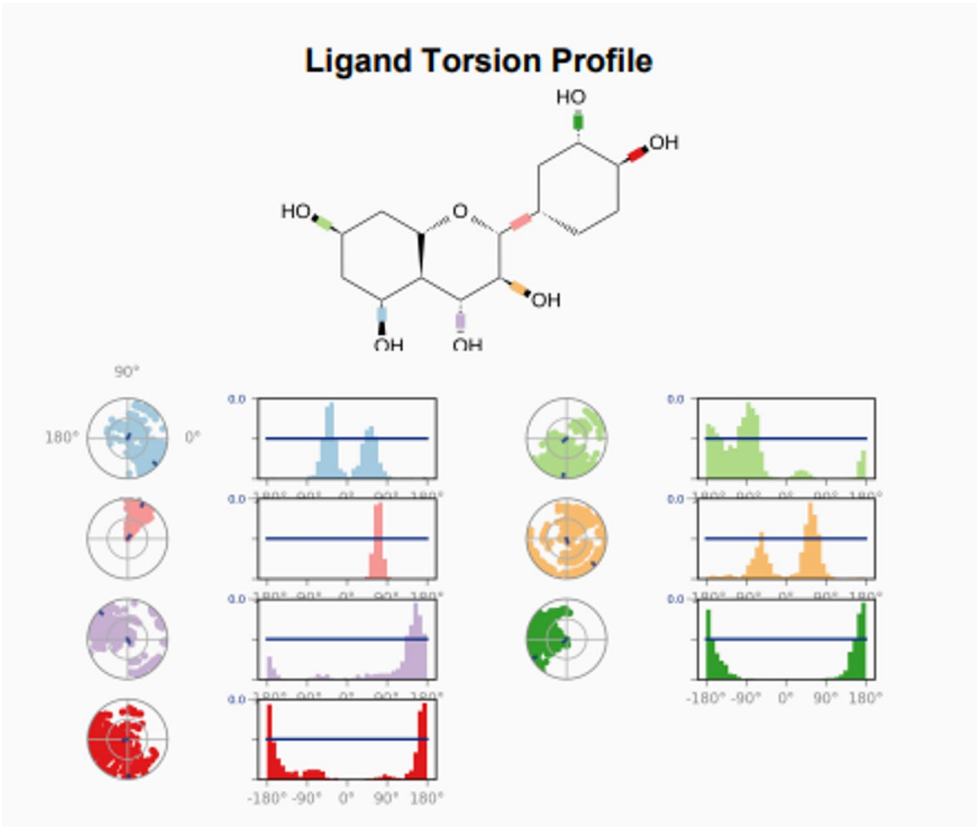

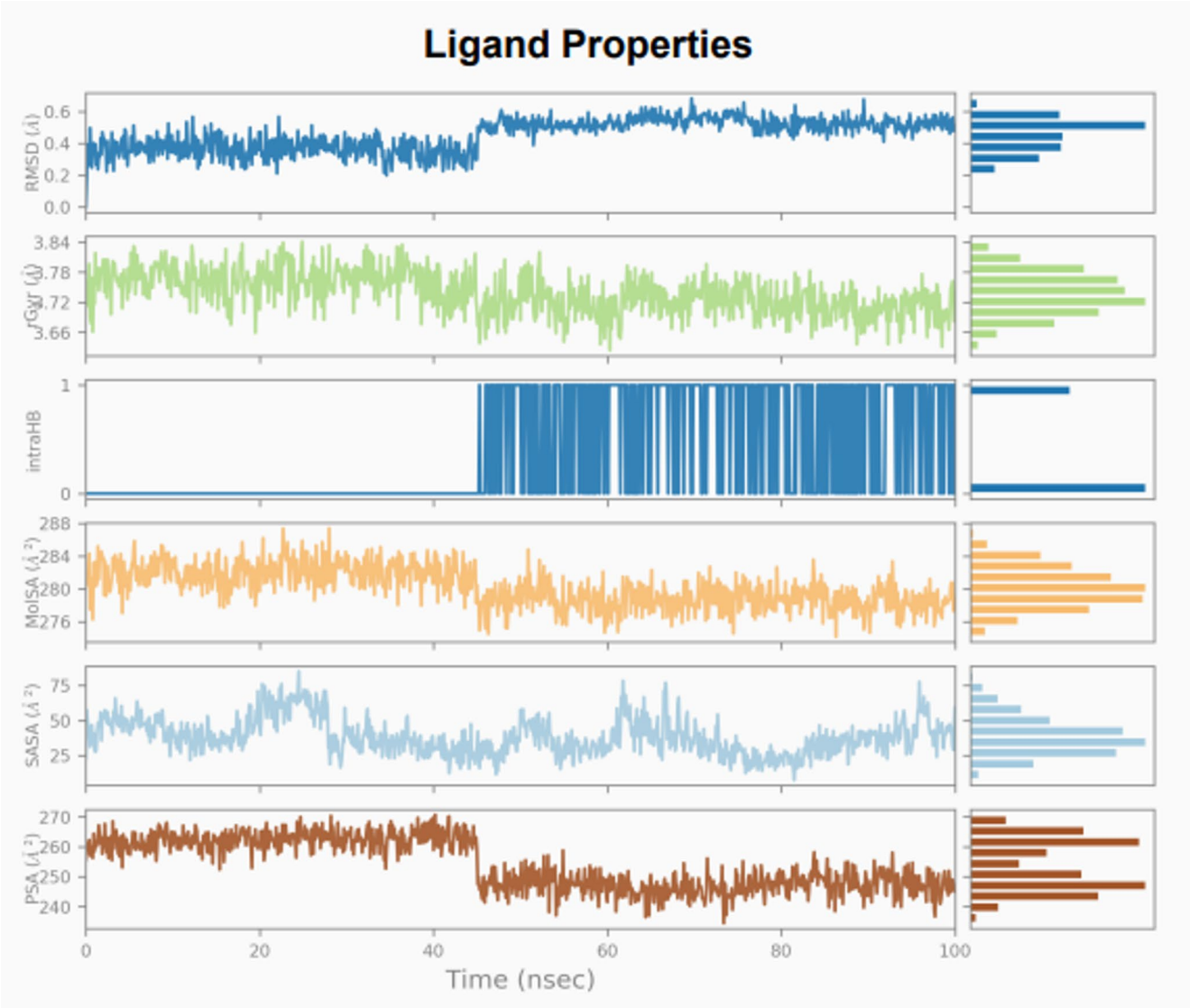


**Fig. 28** Ligand Properties

The quantity of internal hydrogen bonds (HB) that exist within a ligand molecule is known as intramolecular hydrogen bonds (intraHB).

A probe radius of 1.4 Å is used to compute the molecular surface area, or MolSA. This value is equivalent to a van der Waals surface area.

The area of a molecule's surface that a water molecule may reach is known as solvent accessible surface area, or SASA. The Polar Surface Area (PSA): The surface area of a molecule accessible to solvents that is solely provided by nitrogen and oxygen atoms.

### Quercetin as a Stable and Effective Binder

Quercetin maintained a highly stable and consistent binding profile with 17β-HSD Type 1 throughout the simulation. Its strong hydrogen bonding, preserved protein structure, and favorable conformational adaptability underscore its potential as a robust inhibitor. While less hydrophobic than kaempferol, quercetin's superior maintenance of secondary structure and higher polar interaction profile position it as a strong candidate for further therapeutic exploration in hormone-related cancer treatment.

## Comparative Analysis of Kaempferol and Quercetin in Molecular Dynamics Simulation with 17β-HSD Type 1 (PDB ID: 3HB5)

Comparative Analysis of Quercetin Vs. Kaempferol shown in Table 3. According to the results of the molecular dynamics simulation, both kaempferol and quercetin had significant and stable binding to the 17β-HSD Type 1 enzyme, an

**Table 3** Comparative molecular dynamics analysis of quercetin and kaempferol binding with 17β-HSD type 1

| Property | Quercetin | Kaempferol | Implication |
|---|---|---|---|
| Protein RMSD | Stable (~2 Å) | Stable (~2 Å) | Protein conformation remains intact for both. |
| Ligand RMSD | Lower (~1.5 Å) | Lower (~1.5 Å) | Both ligands exhibit strong binding. |
| Hydrogen Bonds | Strong & Consistent | Strong | Quercetin forms slightly stronger H-bond interactions. |
| Hydrophobic Contacts | Moderate | Higher | Kaempferol has stronger hydrophobic interactions. |
| Protein Secondary Structure Stability | 36.83% Helix, 50.08% SSE | 34.87% Helix, 48.00% SSE | Quercetin maintains protein stability slightly better. |
| Binding Energy | ~ −42 kcal/mol | ~ −45 kcal/mol | Kaempferol has slightly stronger binding affinity. |

importantly targeted protein involved in regulation of hormone signaling and the progression of hormone-dependent cancers, including breast cancer, among others. Over the 100 ns simulation, both ligands presented low (RMSD) root-mean-square deviation values around 1.5 Å, indicating low deviation from the active site. In either case, the protein maintained its full three-dimensional conformation, although the quercetin complex maintained secondary structure elements a little better than the kaempferol, indicating a difference in how the two ligands contain the structure of the protein.

For the analysis of the interaction profiles, quercetin formed stronger and more stable hydrogen bonds with residues in the binding site compared to kaempferol. Stable and strong hydrogen bonds would help stabilize the occupancy and dynamic binding behaviour onto the protein target. In addition to having weaker provide that may be less significant than the documented bonding of quercetin, kaempferol did have a larger number of hydrophobic interactions as a part of the binding, including more nonpolar than polar bonded interactions with the hydrophilic regions of the protein targeting. It is plausible that these interactions are part of a different mechanism for stabilization, rather than stabilizing polar interactions involved with water-mediated bridge interactions and were also important non-polar interactions that stabilize the binding pocket requirements of both ligands.

The antioxidant activity of flavonoids quercetin and kaempferol is important to reduce oxidative stress, an important risk factor in carcinogenesis in Fig. 29. These compounds prevent the damage of DNA and hamper tumor development and progression by scavenging reactive oxygen species (ROS). Moreover, their signaling pathway

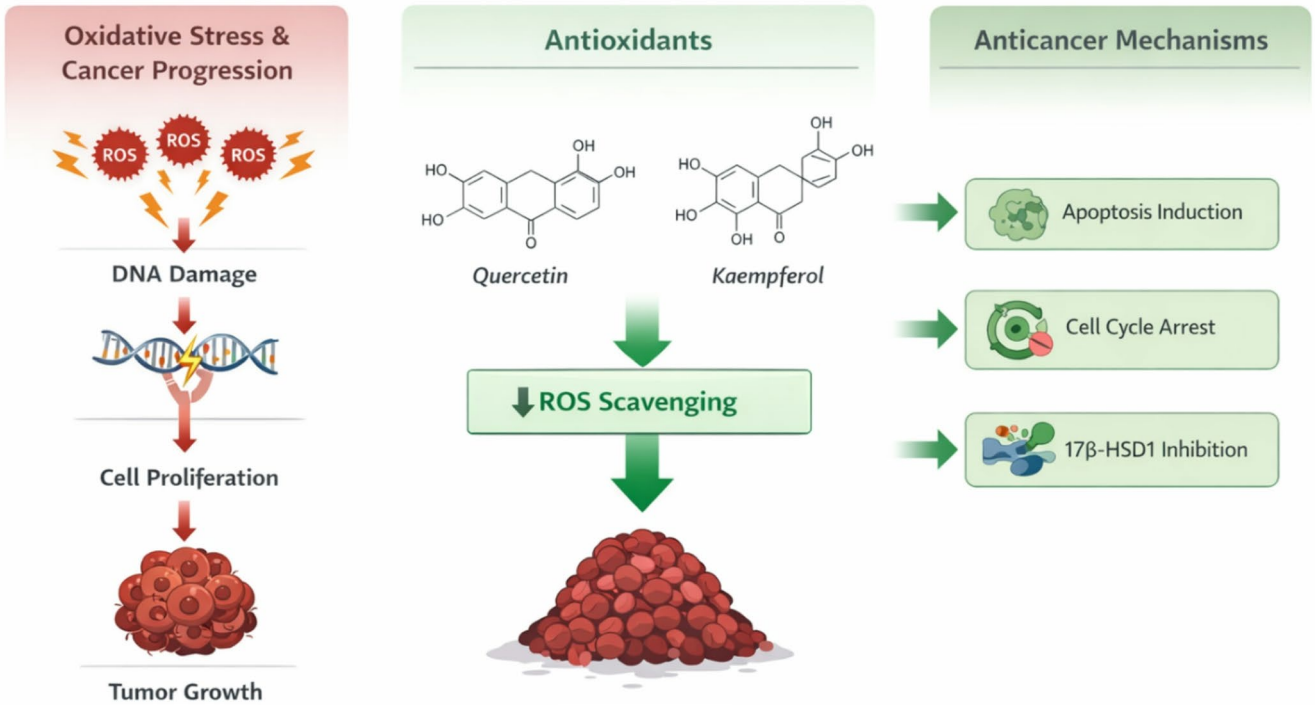


**Fig. 29** Mechanistic Link Between Antioxidant Activity and Anticancer Effects

modulation capabilities related to apoptosis, cell proliferation, and inhibition of enzymes 17 2 HSD1 offer a mechanistic foundation to their anticancer effect.

In spite of the fact that the current research has been able to offer solid computational support to the interaction of quercetin and kaempferol with 17β-HSD1, in-vitro cytotoxicity research is needed to confirm their biological activity. These flavonoids have been reported to have strong cytotoxic effects on different cancer cell lines, which support their therapeutic effects. Thus, the next steps in work will be in-vitro assays to determine a direct correlation between the obtained in silico results and biological activity.

## Limitation

One of the weaknesses of this study is that computational analysis was limited to the major phytoconstituents of selection. A detailed virtual screening of all the phytochemicals reported and experimental assessment would give better insight into the holistic therapeutic potential of the plant. One of the weaknesses of this study is that MM/GBSA binding free energy calculations have not been done, which would give a more reliable ranking of the ligand binding affinity.

## Future scope

Future research will be directed towards large-scale in silico screening of other phytochemicals found in the plant, and then in-vitro and in-vivo screening to determine their cytotoxic effects and therapeutic potential.

## Summary

The present study aimed to comprehensively evaluate bioactive constituents through systematic phytochemical investigation, isolation, and advanced molecular modeling studies. Quantitative phytochemical profiling revealed a high abundance of secondary metabolites, such as phenolics (305 mg/g) and flavonoids (296 mg/g), along with substantial levels of alkaloids, saponins, and tannins, underscoring the therapeutic richness of the plant extract. Guided by preliminary screening, targeted isolation was performed using chromatographic techniques, leading to the purification of the major flavonoids. Structural elucidation of the isolated compounds was accomplished through detailed spectroscopic analyses, confirming their identity as quercetin and kaempferol.

In silico Studies using molecular docking were conducted to assess the capacity for binding of these flavonoids to cancer-related targets especially those in hormone signaling, DNA repair, immune modulation, and apoptosis. Both quercetin and kaempferol had high binding scores on 17β-HSD type 1, HER2, STING, and PARP10, which could indicate anticancer potential for these compounds. Molecular dynamics simulation on the complexes were observed at 100 ns to indicate the stability and dynamics of the ligand-protein complexes. This study showed that both ligands could maintain a stable binding position on 17β-HSD Type 1, where kaempferol had a slightly more negative binding energy due to hydrophobic interactions while quercetin increased the protein stability through solid hydrogen bonding.

This integrative study from quantifying phytochemicals to computational docking provides a strong narrative where isolated flavonoids may be therapeutically relevant, with potential as leads in hormone-regulated cancer therapies.

## Conclusion

This study successfully demonstrated the potential of isolated flavonoids for therapeutic applications through an integrated research framework bringing together quantitative phytochemistry, structural elucidation, simulation studies and molecular docking. This study demonstrated that both quercetin and kaempferol show strong, stable binding to 17β-HSD type 1 and complementary binding. These results support their candidacy as leads for preclinical research targeting hormone-related cancers and show the complementary strength of phytochemical discovery and computational checks.

**Author Contributions** Author 1: Gopika V CShe Performed the Analysis the overall concept, writing and editingAuthor 2: Dr. V Jayashree-She participated in the methodology, Conceptualization, Data collection and writing the study.

**Funding** No fund received for this project.

**Data Availability** No datasets were generated or analysed during the current study.

## Declarations

**Ethical Approval and Human Participation** No ethics approval is required.

**Competing interests** The authors declare no competing interests.

## References

1. Costa GM, Gazola AC, Zucolotto SM, Castellanos L, Ramos FA, Reginatto FH, et al. Chemical profiles of traditional preparations of four South American *Passiflora* species by chromatographic and capillary electrophoretic techniques. Rev Bras Farmacogn. 2016;26(4):451–8. https://doi.org/10.1016/J.BJP.2016.02.005.

2. Nikolova K, Velikova M, Gentscheva G, Gerasimova A, Slavov P, Harbaliev N, et al. Chemical compositions, pharmacological properties and medicinal effects of genus *Passiflora* L.: a review. Plants. 2024;13:228.
3. Akinjagunla AD, 2023 SA, Anandaram H, Karpagavalli MS, Ranjithkumar D. *Cissus quadrangularis* is a potential anticancer herb: a review. Orient J Chem. 2023;39(5):1164–9. https://doi.org/10.13005/ojc/390509.
4. Leal AEBP, Lavor EM, Barbosa JM, Araújo MTMF, Alves CDSC, Oliveira Júnior RG, et al. Pharmacological activities of the genus *Passiflora* (Passifloraceae): a patent review. Curr Top Med Chem. 2022;22(28):2315–28. https://doi.org/10.2174/1568026622666220819160923.
5. Saeki D, Yamada T, Kajimoto T, Muraoka O, Tanaka R. A set of two diastereomers of cyanogenic glycosides from *Passiflora quadrangularis*. Nat Prod Commun. 2011;6(8):1091–4. https://doi.org/10.1177/1934578X1100600810.
6. Hamid HS, Patil S. A phytochemical and pharmacological review of an Indian plant: *Cissus quadrangularis*. Med Sci Forum. 2023;21(1):20. https://doi.org/10.3390/ECB2023-14557.
7. Guerrero MF, Bareño LL, Puebla P, San Feliciano A. Vascular mechanisms of triterpenoid saponins isolated from *Passiflora quadrangularis* L. Vitae. 2020;27(2):1–11. https://doi.org/10.17533/UDEA.VITAE.V27N2A02.
8. Ramaiya SD, Lee HH, Xiao YJ, Shahbani NS, Zakaria MH, Bujang JS. Organic cultivation practices enhanced antioxidant activities and secondary metabolites in Passiflora quadrangularis. PLoS ONE. 2021;16(7).
9. Yanasan N, Natakankitkul S, Kiattisin K, Phupaisan N, Inkongngam S, Wangkananon W. Bioactive content and antioxidant activities of Passiflora quadrangularis fruit extracts for cosmetic applications. Cosmetics Conference Proceedings. 2022:15–23.
10. Castro PCF, Hoshino A, Silva JC, Mendes FR. Possible anxiolytic effect of two extracts of *Passiflora quadrangularis* L. in experimental models. Phytother Res. 2007;21(5):481–4. https://doi.org/10.1002/PTR.2079.
11. Sofiabadi M, Soheili MM, Soleimani P. Effect of *Passiflora* extract on passive avoidance learning and memory in male rats. J Birjand Univ Med Sci. 2019;26(1):13–20. https://doi.org/10.32592/JBIRJANDUNIVMEDSCI.2019.26.1.102.
12. Bareño LL, Puebla P, Guerra CM, San Feliciano A, Isaza G, Guerrero MF. *Passiflora quadrangularis* L. prevents experimental hypertension and vascular remodelling in rats exposed to nitric oxide deficit. Vitae. 2017;24(3):186–95. https://doi.org/10.17533/UDEA.VITAE.V24N3A04.
13. Pareeth CM, Babu TD. Analysis of cytotoxic and antitumor potential of *Passiflora quadrangularis*. J Herbs Spices Med Plants. 2023. https://doi.org/10.1080/10496475.2023.2225147.
14. Amaral RG, Gomes SVF, Luciano MCS, Pessoa CO, Andrade LN, Severino P, et al. Cytotoxic potential of 14 *Passiflora* species against cancer cells. J Med Plants Res. 2019;13(7):157–66. https://doi.org/10.5897/JMPR2019.6744.
15. Yalcin S. Molecular docking, drug likeness, and ADMET analyses of *Passiflora* compounds as P-glycoprotein inhibitor for the treatment of cancer. Curr Pharmacol Rep. 2020;6(6):429–40. https://doi.org/10.1007/S40495-020-00241-6.
16. Lewis B, Herrlinger K, Craig T, Mehring-Franklin CE, DeFreitas Z, Hinojosa-Laborde C. Antihypertensive effect of passion fruit peel extract and its major bioactive components following acute supplementation in spontaneously hypertensive rats. J Nutr Biochem. 2013;24(7):1359–66. https://doi.org/10.1016/J.JNUTBIO.2012.11.003.
17. Cruz JMA, Pereira ZC, Correa RF, Lamarão CV, Sanches EA, Campelo PH, et al. Bioactive compounds, functional properties, and technological application of *Passiflora quadrangularis*: a review. JSFA Rep. 2023;3(4):150–60. https://doi.org/10.1002/jsf2.108.
18. Yuldasheva LN, Carvalho EB, Catanho MTJA, Krasilnikov OV. Cholesterol-dependent hemolytic activity of *Passiflora quadrangularis* leaves. Braz J Med Biol Res. 2005;38(7):1061–70. https://doi.org/10.1590/S0100-879X2005000700009.
19. Ajanal M, Gundkalle MB, Nayak SU. Estimation of total alkaloid in Chitrakadivati by UV-Spectrophotometer. Anc Sci Life. 2012;31(4):198–201. https://doi.org/10.4103/0257-7941.107361.
20. Sultana S, Lawag IL, Lim LY, Foster KJ, Locher C. A critical exploration of the total flavonoid content assay for honey. Methods and Protocols. 2024;7(6):95. https://doi.org/10.3390/mps7060095.
21. Cheok CY, Salman HAK, Sulaiman R. Extraction and quantification of saponins: a review. Food Res Int. 2014;59:16–40. https://doi.org/10.1016/j.foodres.2014.01.057.
22. Łukowski A, Jagiełło R, Robakowski P, Adamczyk D, Karolewski P. Adaptation of a simple method to determine the total terpenoid content in needles of coniferous trees. Plant Sci. 2022;314:111090. https://doi.org/10.1016/j.plantsci.2021.111090.
23. Çilesizoğlu B, Yalçin E, Çavuşoğlu K, Sipahi Kuloğlu S. Qualitative and quantitative phytochemical screening of *Nerium oleander* L. extracts associated with toxicity profile. Sci Rep. 2022;12(1):21421. https://doi.org/10.1038/s41598-022-26087-0.
24. Dokuparthi SK, Reddy TRM. Antioxidant and nephroprotective activity of flavonoid rich fraction of *Alphonsea sclerocarpa* Thw. Int J Pharm Sci Drug Res. 2021;13(4):384–94.
25. Sujatha E, Fatima M. Phytochemical profile, antioxidant and cytotoxic activities of *Landoltia punctata*. Ann Phytomed. 2023;12(1):1–6.
26. Le Bot M, Thibault J, Pottier Q, Boisard S, Guilet D. An accurate, cost-effective and simple colorimetric method for the quantification of total triterpenoid and steroidal saponins from plant materials. Food Chem. 2022;383:132597. https://doi.org/10.1016/j.foodchem.2022.132597.
27. Kumar A, Banerjee N, Singamaneni V, Dokuparthi SK, Chakrabarti T, Mukhopadhyay S. Phytochemical investigations and evaluation of antimutagenic activity of the alcoholic extract of *Glycosmis pentaphylla* and *Tabernaemontana coronaria* by Ames test. Nat Prod Res. 2017. https://doi.org/10.1080/14786419.2017.1318384.
28. Khattab OM, Khalifa SAM, Ghoran SH, Awad HM, Said IG, Aldahmash B, et al. Isolation and structure elucidation of new diterpenoids and triterpenoids from frankincense resin: insights into antimicrobial activity and docking studies. J Mol Struct. 2025;1339:142054. https://doi.org/10.1016/j.molstruc.2025.142054.